Pergamon

Geochimica et Cosmochimica Acta, Vol. 68, No. 7, pp. 1617–1633, 2004

0016-7037/04 $30.00 + .00

doi:10.1016/j.gca.2003.09.010

Melt structural control on olivine/melt element partitioning of Ca and Mn

BJORN O. MYSEN[1,*] and EMILY V. DUBINSKY[2]

[1]Geophysical Laboratory, 5251 Broad Branch Road NW, Washington, DC 20015, USA
[2]Department of Earth and Environmental Science, Stanford University, Stanford, CA 94305, USA

(*Received February* 6, 2003; *accepted in revised form September* 16, 2003)

Abstract—Relationships between mineral/silicate melt partition coefficients and melt structure have been examined by combining Ca and Mn olivine/melt partitioning data with available melt structure information. Compositions were chosen so that melts with olivine on their liquidii range in degree of polymerization, NBO/T, from ~0.5 to ~2.5 under near isothermal conditions (1350–1400°C). Olivine/melt Ca-Mn exchange coefficients, Ca(olivine)/CaO(melt)/MnO(olivine)/MnO(melt) ($K_{D\ Ca\text{-}Mn}^{olivine/melt}$), as a function of melt NBO/T have a parabolic shape with a minimum $K_{D\ Ca\text{-}Mn}^{olivine/melt}$-value at NBO/T near 1. Notably, published $K_{D\ Fe2^{+}\text{-}Mg}^{olivine/melt}$ versus NBO/T functions are also parabolic with a maximum in $K_{D\ Fe2^{+}\text{-}Mg}^{olivine/melt}$ near 1 (Kushiro and Mysen, 2002).

The olivine/melt partitioning data are modeled in terms of structural units (Q^n-species) in the melt. The NBO/T-value corresponding to the minimum $K_{D\ Ca\text{-}Mn}^{olivine/melt}$ is near that where the abundance ratio of Q^n-species, X_{Q3}/X_{Q2}, has its largest value. Therefore, the activity coefficient ratio in the melt, $\gamma_{Ca2^{+}}(melt)/\gamma_{Mn2^{+}}(melt)$, attains a minimum where the abundance ratio of X_{Q3}/X_{Q2} is at maximum. It is inferred from this relationship that Ca^{2+} in the melts is dominantly bonded to nonbridging oxygen (Ca-NBO) in Q^3-species, whereas Mn^{2+} is bonded to nonbridging oxygen (Mn-NBO) in less polymerized Q^n-species such as Q^2. *Copyright © 2004 Elsevier Ltd*

1. INTRODUCTION

A fundamental process characterizing igneous petrogenesis is major, minor, and trace element partitioning between minerals and silicate melt. The element solution behavior in minerals and melts governs the partitioning behavior. Crystal structure governs major element solution behavior. Structural models for minor and trace element solution in crystals have utilized crystallographic features such as defect concentration and lattice strain energy (e.g., Iiyama and Volfinger, 1976; Blundy and Wood, 1994; Wood and Blundy, 2001).

Melt composition also exerts an influence on element partitioning. Empirical models that describe relationships between partitioning behavior and melt composition have been suggested (e.g., Watson 1976, 1977; Hart and Davis, 1978; Colson et al., 1988; Jurewicz and Watson, 1988; Kohn and Schofield, 1994; Libourel, 1999; Jaeger and Drake, 2000; Walter, 2001; Toplis and Corgne, 2002). Most of these models do not consider how the structural behavior of the elements in the melt affect their solubility behavior and, therefore, mineral/melt partitioning. An exception to this generalization is the study by Kohn and Schofield (1994) who suggested that steric hindrance in the melt might govern the relative stability of metal-oxygen bonds.

Empirical variables proposed to quantify relations between melt composition and element partitioning include concentrations of alkali metals, alkaline earths, and Si/O ratio of the melt (e.g., Watson, 1977; Hart and Davis, 1978; Jurewicz and Watson, 1988; Libourel, 1999; Wood and Blundy, 2001). The degree of polymerization of a silicate melt, NBO/T,[1] is another of such proposed variables (e.g., Mysen and Virgo, 1980; Jaeger and Drake, 2000; Kushiro and Walter, 1998, Kushiro and Mysen, 2002). The NBO/T parameter has a melt structure connotation because NBO/T of a melt can be calculated from bulk composition provided that the structural roles of the major elements in the melt are known. Available melt structure data are sufficient to calculate the NBO/T of silicate melts in this manner at ambient pressure and in the absence of volatiles (see Mysen, 1988, for discussion of NBO/T calculation of silicate glasses and melts).

When relating mineral/melt partition coefficients to NBO/T of melt, it is assumed that a principal melt structural control on partition coefficients is the activity of nonbridging oxygen because the activity of nonbridging oxygen, a_{NBO}, is correlated with NBO/T. The NBO/T is not, however, a quantitative measure of a_{NBO} because the nonbridging oxygens in coexisting Q^n-species[2] in melts most likely are energetically nonequivalent. The a_{NBO} depends on the electronic properties of the network-modifying cations bonded to nonbridging oxygen, on the Al/Si-ratio, and on $Si^{4+} \Leftrightarrow Al^{3+}$ ordering in the melts (Mysen, 1990). So, although empirical expressions relating NBO/T to mineral/melt partition coefficients have been somewhat successful at least over comparatively narrow NBO/T-intervals, it should be pointed out that three implicit assump-

* Author to whom correspondence should be addressed (mysen@gl.ciw.edu).

[1] NBO/T denotes the number of nonbridging oxygen, NBO, per tetrahedrally coordinated cation, T. A nonbridging oxygen, NBO, is an oxygen bonded to both a tetrahedrally coordinated cation and a cation in another coordination state. A bridging oxygen, BO, is bonded to two tetrahedrally coordinated cations. In most silicate melts relevant to magmatic processes, the dominant T-cations are Si^{4+} and Al^{3+} although minor components such as P^{5+} and Ti^{4+} can also exist in tetrahedral coordination. Ferric iron in highly oxidized melts can also occur in IV-fold coordination with oxygen. These latter three cations tend to form Si-free tetrahedral clusters, whereas Al^{3+} normally substitutes for Si^{4+} (see Mysen, 1990, for a detailed review of these structural features).

[2] The Q^n-notation is used to define species in silicate melts whose number of bridging oxygen, n, differ. In most silicate melts, n = 0, 1, 2, 3, and 4. The number of nonbridging oxygen equals 4-n.

Table 1. Normal composition of starting materials (wt%).[a]

	FLQ1MC[b]	FLQ2MC[b]	FNQMC[b]	FAQ1MC[b]	FAQ2MC[b]	FDAQMC[b]	FDMC[b]	FDAk.5MC[b]	FDAkMC[b]	FDMC-1[c]	FDMC-2[c]	FDMC-3[c]	FDAkMC-1[c]	FDAkMC-2[a]	FDAkMC-3[c]
SiO_2	55.44	57.14	45.13	44.89	47.32	46.74	46.2	45.41	44.61	46.2	46.2	46.2	44.61	44.61	44.61
Al_2O_3	13.14	6.04	7.5	18.1	10.03	5.03	0	0	0	0	0	0	0	0	0
FeO(T)	3.05	5.5	6.37	5.8	7.47	7.25	6.91	5	4.21	6.91	6.91	6.91	4.21	4.21	4.21
MnO	0.95	0.95	0.95	1	1	1	1	1	1	1	1	1	1	1	1
MgO	10.29	19.78	30.5	19.26	27.69	30.54	33.47	29.35	25.23	33.47	33.47	33.47	25.23	25.23	25.23
CaO	5	5	5.00	9.96	5.51	8.45	11.43	17.69	23.95	8	5	2	18	13	8
Na_2O	0	0	4.55	0	0	0	0	0	0	3.43	6.43	9.43	5.95	10.95	15.95
K_2O	12.77	5.58	0	0	0	0	0	0	0	0	0	0	0	0	0

[a] FeO(T): Total iron as FeO.
[b] One of the nine base compositions (see text for discussion).
[c] One of compositions used for examination of effect of Na/Ca (see text for discussion).

tions have not been evaluated. It is assumed that (i) the partition coefficients depend on the activity of nonbridging oxygens in the melt, (ii) that NBO/T can be used as an expression of this activity, and (iii) that there is no ordering of the elements of interest among structural positions in the melt. Because most elements of geochemical interest are network-modifiers in silicate melts, their solution behavior in depends on the activity of nonbridging oxygen, $a_{NBO.}$ However, NBO/T is not equivalent to a_{NBO}. Ryerson (1985) found from analysis of liquidus phase relations in metal oxide-silica systems that the activity of SiO_2 in melts depends not only on metal/silicon ratio, but also on the ionization potential of the metal. It is, therefore, likely, that the activity of other components such as nonbridging oxygen also varies with Si/O-ratio and with ionization potential of the metal cation. The ordering of alkalis and alkaline earths among energetically nonequivalent nonbridging oxygen may also affect the activity of nonbridging oxygen. Ordering of alkaline earth and alkali metals among energetically nonequivalent nonbridging oxygens in alkali and alkaline earth silicate glasses has been documented (see, for example, Jones et al., 2001; Lee et al., 2002; Lee and Stebbins, 2003). The extent of cation ordering among the nonbridging oxygen is a function of the electronic properties of the metal cation (e.g., Lee and Stebbins, 2003).

In modeling mineral/melt element partitioning relevant to igneous processes, therefore, the utility of correlating NBO/T with mineral/melt partition coefficients is not clear. An alternative to this approach is to assess how individual elements may occupy specific structural positions in silicate melts, and to consider mineral/melt partitioning behavior in this light. Examination of these latter relationships is the principal purpose of this report.

2. EXPERIMENTAL METHODS

Olivine/melt partitioning was employed to examine how melt composition and melt structure may govern partitioning behavior. In silicate melts, ionic radius is a critical factor governing the interaction of network-modifying cations with nonbridging oxygen (e.g., Mysen, 1999; Lee and Stebbins, 2003). To this end, olivine/melt partitioning of Ca^{2+} and Mn^{2+} was studied. The ionic radii of Ca^{2+} and Mn^{2+} differ by ~25% (Whittaker and Muntus, 1970). Different structural roles of these two cations in the melts are, therefore, likely. Calcium and Mn are minor components in olivine. Olivine/melt partition coefficients are not likely dependent on the Ca and Mn solution behavior in olivine in the concentration range examined here (see further discussion of this question below). Thus, composition-dependent variation in Ca and Mn olivine/melt partition coefficients are likely to reflect their solution behavior in the melt.

The starting materials were 9 mixtures in the systems forsterite-fayalite-leucite-quartz, forsterite-fayalite-nepheline-quartz, forsterite-fayalite-anorthite-quartz, forsterite-fayalite-diopside-anorthite-quartz, and forsterite-fayalite-diopside-akermanite (Table 1). One wt% MnO was added to all starting compositions.

These starting compositions were chosen to cover a wide range of melt polymerization where olivine is the liquidus phase at nearly constant temperature. A wide range of melt polymerization optimizes the range in Q^n-species abundance, which is important for examination of cation interaction with nonbridging oxygen in specific types of Q^n-species in the melt. By using appropriate compositions in these systems (Table 1), olivine is a liquidus phase coexisting with melts in the NBO/T-range ~0.5 to ~2.5 at nearly constant temperature (1350–1400°C; Kushiro and Mysen, 2002). This range in NBO/T of the melt offers the possibility to evaluate relations between ordering of network-modifying cations among energetically nonequivalent nonbridging oxygen and olivine/melt element partitioning under nearly isothermal conditions.

In the 9 compositions chosen, Ca, Mg, Fe^{2+} and possibly Na and K may be network-modifying cations and could, thus, form bonding with nonbridging oxygen in the melts. However, the melts in equilibrium with olivine in these systems have (Na + K) ≤ Al. Therefore, alkali metals will not serve as network-modifiers, but instead serve to charge-balance Al^{3+} in tetrahedral coordination, whereas Ca, Mg, and Fe^{2+} remain at least in part as network-modifying cations.[3] These relationships exist because among alkali- and alkaline earth–charge-balanced aluminates in silicate melts, their relative stabilities are K > Na > Ca > Mg (see, for example, Navrotsky et al., 1985; Navrotsky, 1995). As a result, in experiments with these 9 base compositions on Ca, Mg, and Fe^{2+} (when present) are network-modifying cations and may compete for available nonbridging oxygen sites in the melts.

To obtain additional information on possible effects of Na^+ as a network-modifying cation on olivine/melt element partitioning behavior, two starting compositions based on FDMC and FDAkMC were prepared. In these compositions, Na was exchanged with Ca to examine Na/Ca as a principal composition variable (compositions FDMC-1, −2, and −3, and FDAkMC-1, −2, and −3 in Table 1). These compositions were prepared because structural data for Na_2O-SiO_2 and CaO-SiO_2 melts at high temperature indicate that Na-NBO (NBO, nonbridging oxygen) are more stable than Ca-NBO bonds where the difference in relative stability is more pronounced the more polymerized the NBO-bearing Q^n-species (see Mysen, 1995, 2003, for review of such structural data). Thus, variations in Na/Ca likely affect the activity coefficients of all network-modifying cations in the melts. Such variations, in turn will affect mineral/melt partitioning behavior.

Starting materials were made from mixtures of oxides together with $CaCO_3$, Na_2CO_3, and K_2CO_3. These mixtures (~1 g each) were ground under alcohol in an agate mortar for 1 h, heated to 1500°C for 1 h in iron-saturated Pt crucibles to form melts or melt + olivine mixtures, and then quenched. These materials were then ground to ≤20 μm to be used as starting materials.

The experimental charges were contained in $Pt_{95}Au_5$ envelopes and

[3] The concentration of Fe^{2+} likely is quite low in most experiments because these were conducted in air (see also below). Thus, Ca and Mg are the dominant network-modifying cations in melts in equilibrium with olivine from these nine compositions.

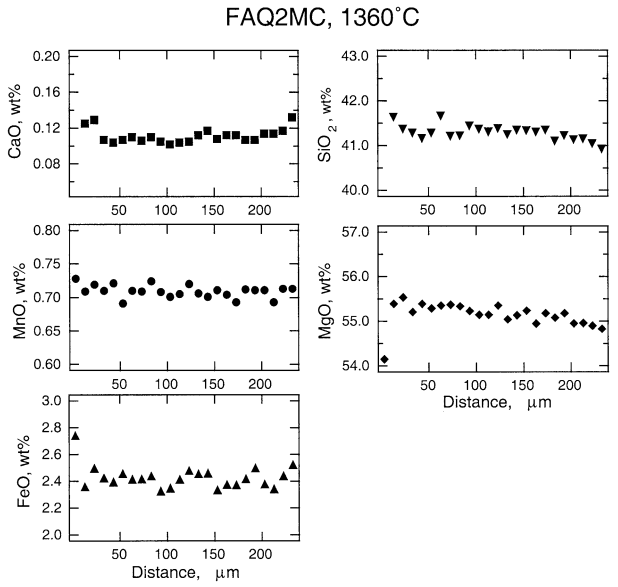

Fig. 1. Electron microprobe traverses from rim to rim across olivine from experiment as indicated on diagram.

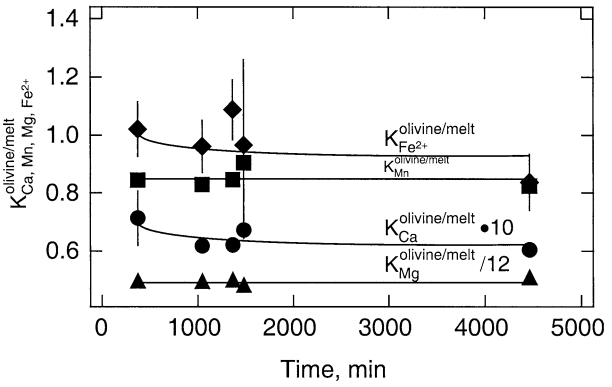

Fig. 2. Partition coefficients for Ca, Mn, Mg, and Fe^{2+} (wt% oxide olivine/wt% oxide melt) as a function of experimental duration (data from Table 3).

subjected to experimental temperatures in $MoSi_2$-heated vertical quench furnaces. Most experiments were carried out in air. At the oxygen fugacity (f_{O2}) of air, iron solubility in $Pt_{95}Au_5$ is negligible (Osborn and Arculus, 1975). Selected experiments were also conducted at lower f_{O2} to evaluate (i) relations between Fe^{3+}/Fe^{2+} and mineral/melt partition coefficients, and (ii) to asses whether Mn exists in more than one oxidation state in melts at the high f_{O2} of air. In these experiments, the f_{O2} was controlled with CO/CO_2 gas mixing with an yttria-stabilized ZrO_2-cell to monitor the f_{O2} (e.g., Sato, 1972). In the low f_{O2}-experiments, the samples were suspended on a 100-μm-diameter Pt wire loop with sample/Pt mass ratio between 50 and 100 to minimize Fe-loss to the Pt-loop.

All experimental charges were quenched in water. Typical charges consisted of euhedral olivine, ranging from 10 to 100 μm across, and glass representing quenched silicate liquid.

The crystals and glass were analyzed with a JEOL 8900 electron microprobe operating at 15 kV with 10 nAmp beam current with 30 s counting time. For olivine crystals, analysis was carried out on 3 spots on at least 5 different olivine grains per charge. Glass was analyzed by rastering the electron beam over 10 μm $\times$ 10 μm squares.

The apparent CaO content of olivine near olivine/glass interfaces may be affected by the CaO in glass adjacent to olivine (e.g., Jurewicz and Watson, 1988). This is a potential problem because of the low CaO concentration in olivine (<1 wt% CaO) compared with that of the glass (wt% $CaO^{olivine}$/wt% CaO^{glass} typically is less than 0.1). Analytical traverses across olivine grains grown exceptionally large for this purpose (>100 μm) were employed to assess the minimum distance from olivine/glass boundaries from which reliable CaO analysis of olivine can be obtained. The minimum distance below which interference from the Ca in neighboring glass occurs, appears to be $\leq$20 μm (Fig. 1).

Experimental run duration was approximately 17 to 24 h, except for time studies, which were conducted for 6–72 h (Fig. 2). Partition coefficients reach constant values for durations exceeding 17 h. Experimental durations of 17–24 h, used in most of the present experiments, were, therefore, considered sufficient to reach equilibrium.

The redox ratio of iron can affect the melt structure significantly because Fe^{3+} and Fe^{2+} may occur in structurally different positions in the melt (e.g., Dingwell and Virgo, 1988; Mysen and Virgo, 1989). Partition coefficients may, therefore, depend on the redox ratio of iron in the melt. Mössbauer spectroscopy was used to determine $Fe^{3+}/\Sigma Fe$ and the structural position of Fe^{2+} and Fe^{3+} in the quenched melts (glass). To this end, 11 glasses with the composition of melts coexisting with olivine at 1375–1400°C from starting compositions FLQ1MC, FLQ2MC, FNQMC, FDAQMC, FAQ1MC, FAQ2MC, FDMC, and FDAkMC were prepared for ^{57}Fe resonant Mössbauer spectroscopy. These compositions were made from oxide mixtures and carbonates in the same manner as the other starting compositions above. These glasses were melted at 1375–1400°C (near the temperature at which these melts were formed in the partitioning experiments) and quenched to glass in water. Mössbauer spectroscopy was carried out with a ~1 cm^2 diameter ^{57}Co source with nominal activity of 40 mCi and using constant acceleration. The system was calibrated with Fe foil. All hyperfine parameters are reported relative to metallic Fe.

Most of the Mössbauer spectra were recorded at 298 K. A few spectra were also obtained at 150 K to (i) ascertain the extent to which the recoil-free fraction of Fe^{3+} and Fe^{2+} differs, (ii) to achieve better resolution of the absorption doublets, and (iii) to ascertain in more detail whether or not Fe^{3+} is in tetrahedral or octahedral coordination in these glasses (see Virgo and Mysen, 1985; Alberto et al., 1996; Wilke et al., 2002, for detailed discussion of these issues). For all but the most reduced glass (glass from starting composition FDMC at $f_{O2} = 10^{-9}$ bar at 1375°C) the spectra were fitted to one Lorentzian absorption doublet each for Fe^{3+} and Fe^{2+}, respectively (Fig. 3). There is an ~8% difference in Fe^{3+}/Fe^{2+} calculated from spectra obtained at 298 and 150 K. This difference is consistent with a small difference in recoil-free fraction between Fe^{3+} and Fe^{2+}. For composition where spectra were obtained at 298 K only, the $Fe^{3+}/\Sigma Fe$-values used in NBO/T calculations were corrected with this 8% difference in recoil-free fraction of Fe^{2+} and Fe^{3+} in the glasses.

3. RESULTS AND DISCUSSION

3.1. NBO/T of Melts and the Redox Ratio of Iron

Available structural data for ambient-pressure, iron-free silicate and aluminosilicate glass and melt are sufficient to calculate their NBO/T (degree of polymerization of the silicate network) from their major-element composition (see Mysen, 1988, 1990, 1995, for discussion and review of these data and NBO/T calculations). For Fe-bearing glasses and melts, additional information needed to calculate their NBO/T is $Fe^{3+}/\Sigma Fe$ and the structural behavior of Fe^{2+} and Fe^{3+}. The $Fe^{3+}/\Sigma Fe$ and the structural roles of Fe^{2+} and Fe^{3+} depend on bulk composition of the melt (including Fe content), temperature, and oxygen fugacity (Mysen, 1990). These data were obtained from the Mössbauer spectra of the iron-bearing melts.

An example of a Mössbauer spectrum of glass, quenched from melt equilibrated in air, is shown in Figure 3 with detailed data from all the Mössbauer experiments summarized in Table 2. For all glasses prepared by quenching melt equilibrated with

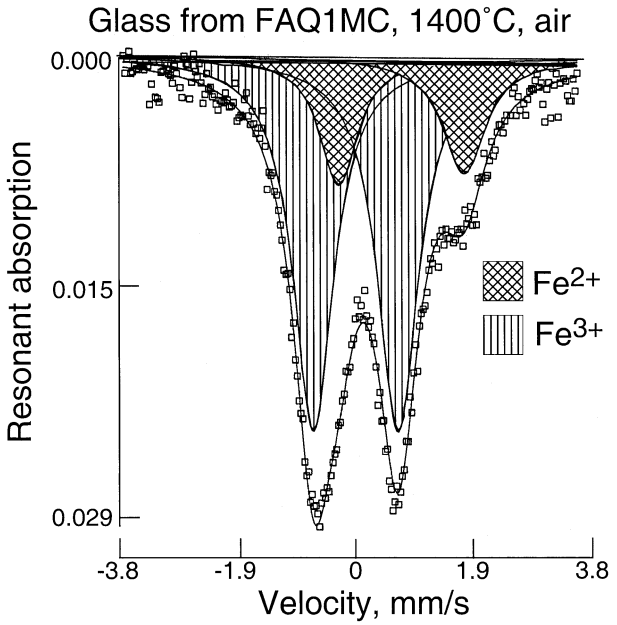

Fig. 3. Example of ^{57} Fe Mössbauer spectrum obtained on glass quenched from melt corresponding to that in equilibrium with olivine for starting composition FAQ1MC in air at 1400°C.

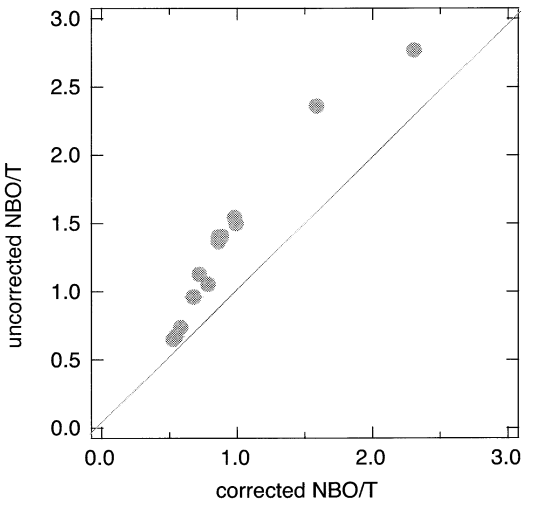

Fig. 4. Comparison of NBO/T of melts in equilibrium with olivine at 1350–1400°C in air calculated under the assumption of all Fe as FeO (uncorrected NBO/T) and with FeO and Fe_2O_3 contents and structural position of Fe^{2+} and Fe^{3+} of the melts from Mössbauer spectroscopy (corrected NBO/T).

air, the Fe^{3+} doublet dominates the spectra resulting in $Fe^{3+}/\Sigma Fe$ between 0.77 and 0.91 depending on composition (Table 2). The hyperfine parameters are consistent with Fe^{2+} being a network-modifying cation (VI-fold coordination with oxygen) and Fe^{3+} a network-former (IV-fold coordination with oxygen) (Virgo and Mysen, 1985). The effect of this structural information on NBO/T of the melts compared with the NBO/T calculated with the assumption that all iron could be considered as a network-modifier is illustrated in Figure 4. The difference between the two NBO/T-values (corrected and uncorrected NBO/T) varies with NBO/T and iron content and can reach as much as 25% (Fig. 4).

Mössbauer spectra were also obtained for glasses from olivine/melt partitioning at reduced f_{O2} (starting composition FDMC was used in these experiments). In the Mössbauer spectra of such glasses, with decreasing f_{O2} the intensity of the Fe^{3+} doublet decreases and that of the Fe^{2+} increases resulting in decreasing $Fe^{3+}/\Sigma Fe$ (Fig. 5A). With decreasing $Fe^{3+}/\Sigma Fe$, the resolution of the Fe^{3+} and Fe^{2+} doublets also becomes less clear. This resolution problem was partially overcome by recording the Mössbauer spectra at cryogenic temperatures (150 K) (quadrupole splitting and isomer shifts increase as systematic functions of decreasing spectral acquisition temperature

Table 2. Summary of Mossbauer parameters from spectra for compositions indicated.

Sample	Composition[a]	Temp. (°C)	log f_{O2}	ISFe^{3+} [b] (mm/s)	QSFe^{3+} (mm/s)	ISFe^{2+} (mm/s)	QSFe^{2+} (mm/s)	$Fe^{3+}/\Sigma Fe$
EVD4gl[c]	FLQ2MC	1400	−0.68	0.281 (9)	1.288 (9)	1.02 (4)	2.01 (4)	0.82 (3)
EVD4gl[c]	FLQ2MC	1400	−0.68	0.365 (6)	1.303 (6)	1.10 (2)	2.11 (2)	0.81 (2)
EVD2gl	FLQ1MC	1400	−0.68	0.28 (2)	1.24 (2)	1.01 (5)	1.92 (5)	0.76 (4)
EVD5gl	DNQMC	1400	−0.68	0.272 (6)	1.256 (6)	1.00 (3)	2.09 (3)	0.91 (2)
EVD9gl	FAQ2MC	1400	−0.68	0.296 (7)	1.358 (7)	1.03 (2)	2.04 (2)	0.78 (2)
EVD14gl	FDAQMC	1400	−0.68	0.292 (6)	1.301 (6)	1.02 (2)	2.04 (2)	0.82 (2)
EVD15gl	FDMC	1400	−0.68	0.296 (6)	1.236 (6)	1.02 (2)	2.03 (2)	0.84 (2)
EVD21gl	FDAkMC	1400	−0.68	0.296 (7)	1.256 (7)	1.01 (3)	2.03 (3)	0.85 (2)
EVD21gl[c]	FDAkMC	1400	−0.68	0.379 (6)	1.282 (6)	1.13 (2)	2.14 (2)	0.84 (1)
EVD8gl	FAQ1MC	1400	−0.68	0.29 (1)	1.37 (1)	1.02 (5)	2.02 (5)	0.77 (3)
EVD56gl	FDMC	1375	−3	0.35 (1)	1.16 (1)	1.04 (2)	1.97 (2)	0.46 (2)
EVD56gl[c]	FDMC	1375	−3	0.41 (1)	1.20 (1)	1.13 (5)	2.11 (5)	0.43 (2)
EVD58gl	FDMC	1375	−5	0.38 (4)	1.017 (4)	1.053 (8)	1.978 (8)	0.23 (2)
EVD58gl[c]	FDMC	1375	−5	0.44 (2)	1.22 (2)	1.153 (5)	2.110 (5)	0.16 (1)
EVD59gl[d]	FDMC	1375	−9	1.03 (2)	2.26 (2)	1.12 (1)	1.88 (1)	0.000
EVD59gl[a]	FDMC	1375	−9	1.19 (2)	2.62 (2)	1.20 (1)	2.03 (1)	0.000

[a] Composition of starting material to form melt composition for which Mossbauer data were obtained (see Table 3 for actual melt compositions).
[b] Hyperfine parameters relative to those of Fe metal.
[c] Spectrum obtained at 150 K.
[d] Mossbauer spectrum of this composition is consistent with no Fe^{3+} and possibly two average Fe^{2+}-oxygen polyhedra (identified as 1 and 2).

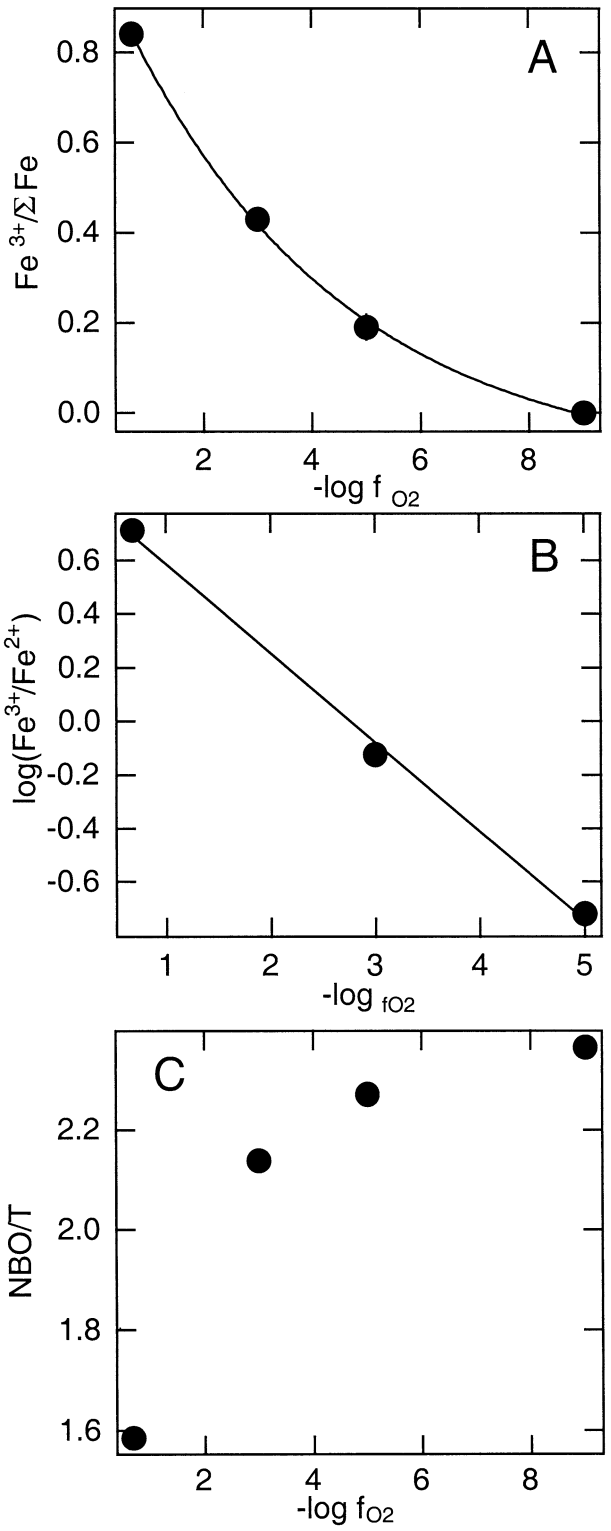

Fig. 5. Redox state of iron in glass with composition corresponding to that coexisting with olivine from starting composition FDMC at 1375°C as a function of oxygen fugacity (log f_{O2}). A. $Fe^{3+}/\Sigma Fe$ as function of $-\log f_{O2}$. B. log (Fe^{3+}/Fe^{2+}) versus $-\log f_{O2}$. C. NBO/T of these melts calculated as a function of log f_{O2} from bulk composition and Mössbauer data on redox state of iron and structural roles of Fe^{3+} and Fe^{2+} in the glass (quenched melt).

thus leading to better resolution of Mössbauer spectra of iron-bearing glasses; Virgo and Mysen, 1985).

The hyperfine parameter values from the Mössbauer spectra of glasses quenched from melts equilibrated in air and at $f_{O2} = 10^{-3}$ bar, are consistent with IV-fold coordinated Fe^{3+} and VI-fold coordinated Fe^{2+} (and, presumably, their melts) as these values compare well with those of crystalline compounds with IV-fold coordinated Fe^{+} and VI-fold coordinated Fe^{2+} (e.g., Annersten, 1976; Waychunas and Rossman, 1983). This conclusion is also consistent with data from glasses where other spectroscopic techniques suggest IV-fold coordinated Fe^{3+} (Calas et al., 1980; Fox et al., 1982; Calas and Petiau, 1983). The Mössbauer spectrum of glass from melt coexisting with olivine from starting composition FDMC equilibrated at 1375°C and $f_{O2} = 10^{-5}$ bar yields hyperfine parameters (Table 2), in particular isomer shift values, intermediate between those of IV- and VI-fold coordinated Fe^{3+} in crystalline materials (e.g., Annersten and Olesch, 1978; Amthauer et al., 1980 see also Virgo and Mysen, 1985). These intermediate values could be interpreted either as due to the existence of Fe^{3+} in mixed coordination states (e.g., Dingwell and Virgo, 1987, 1988) or due to the existence highly distorted Fe^{3+} (IV)-O polyhedra in the glass (Spiering and Seifert, 1985). Although these two alternative structural interpretations will result in slightly different NBO/T-values of the melt, the total amount of Fe_2O_3 is so small in this melt (1.2 wt%) that the effect of using either of these two structural interpretations for Fe^{3+} on the NBO/T of the melt is not large. Because of the uncertainty in the structural assignment of Fe^{3+} and the small effect on NBO/T because of the low ferric iron content, for simplicity, we assume tetrahedrally coordinated Fe^{3+} for the purpose of calculating the NBO/T of this melt.

The relationship between log f_{O2} and log(Fe^{3+}/Fe^{2+}) is linear with a slope near 0.33 (Fig. 5B), similar to the slope for other Fe-bearing alkaline earth silicate and aluminosilicate glasses (Mysen et al., 1984, 1985). The effect of oxygen fugacity (and, therefore, $Fe^{3+}/\Sigma Fe$) on NBO/T of melts in equilibrium with olivine at 1375°C from the FDMC starting composition, calculated from the $Fe^{3+}/\Sigma Fe$ and the structural interpretation of the hyperfine parameters (Fe^{3+} in IV-fold and Fe^{2+} in VI-fold coordination), is shown in Figure 5C.

The redox ratio of iron affects the NBO/T of the melts. For example, for the iron content of melts from composition FDMC at 1375°C (which contains 10.13 wt% iron as iron oxide), the reduction of f_{O2} and, therefore, reduction of $Fe^{3+}/\Sigma Fe$ from 0.81 at $f_{O2} = 10^{-0.68}$ bar (air) to $Fe^{3+}/\Sigma Fe = 0$ at $f_{O2} = 10^{-9}$ bar results in an NBO/T increase from 1.59 to 2.36 (Fig. 5C; Tables 3 and 5). Intermediate f_{O2}-values result in NBO/T-values intermediate between the two extremes (Fig. 5C).

For those melt compositions for which direct determination or redox ratio of iron was not carried out, their $Fe^{3+}/\Sigma Fe$ was estimated. One approach to this estimate is the empirical algorithm of Kilinc et al. (1983). However, a comparison of $Fe^{3+}/\Sigma Fe$ thus calculated and $Fe^{3+}/\Sigma Fe$ determined by Mössbauer spectroscopy yields poor agreement (Fig. 6). The $Fe^{3+}/\Sigma Fe$ calculated with the Kilinc et al. (1983) algorithm consistently is lower than the actual values. This disagreement most likely is because the present glass compositions are considerably outside the composition range used in the development of the

Table 3. Chemical analyses of run products from the 9 basic starting compositions (wt%).[a]

Run no.	EVD2		EVD4		EVD5		EVD6		EVD7		EVD8		EVD9	
Sample	FLQ1MC		FLQ2MC		FNQMC		FNQMC		FNQMC		FAQ1MC		FAQ2MC	
Temp. (°C)	1350		1350		1350		1350		1380		1360		1360	
$-\log f_{O2}$	0.68		0.68		0.68		0.68		0.68		0.68		0.68	
Time (min)	1325		1305		1345		4460		4465		1300		1295	
	Olivine (15)[b]	Glass (3)	Olivine (15)	Glass (3)	Olivine (15)	Glass (3)	Olivine (15)	Glass (3)	Olivine (15)	Glass (3)	Olivine (15)	Glass (3)	Olivine (15)	Glass (3)
SiO_2	41.9 ± 0.9	55.1 ± 0.5	41.8 ± 0.5	59.0 ± 0.6	41.7 ± 0.1	47.1 ± 0.5	41.8 ± 0.2	56.4 ± 0.2	41.9 ± 0.3	47.2 ± 0.1	41.8 ± 0.2	44.6 ± 0.2	41.9 ± 0.2	49.96 ± 0.07
Al_2O_3		12.8 ± 0.2		6.96 ± 0.09		12.0 ± 0.1		12.4 ± 0.1		11.20 ± 0.01		17.85 ± 0.01		13.03 ± 0.03
FeO	0.84 ± 0.09	3.26 ± 0.09	1.78 ± 0.04	6.22 ± 0.05	1.56 ± 0.04	9.62 ± 0.07	0.78 ± 0.04	3.61 ± 0.05	1.63 ± 0.03	8.81 ± 0.09	1.49 ± 0.03	5.91 ± 0.07	2.45 ± 0.09	9.02 ± 0.01
MnO	1.10 ± 0.02	0.88 ± 0.02	0.92 ± 0.01	0.939 ± 0.005	0.86 ± 0.01	1.021 ± 0.003	1.34 ± 0.01	0.958 ± 0.007	0.76 ± 0.01	1.05 ± 0.02	0.663 ± 0.007	0.971 ± 0.004	0.693 ± 0.009	1.130 ± 0.001
MgO	56.5 ± 0.2	9.2 ± 0.2	55.5 ± 0.3	12.81 ± 0.1	56.0 ± 0.3	14.05 ± 0.03	55.4 ± 0.4	8.88 ± 0.05	55.0 ± 0.3	16.70 ± 0.04	56.1 ± 0.2	18.1 ± 0.1	54.7 ± 0.3	18.87 ± 0.07
CaO	0.401 ± 0.008	6.0 ± 0.2	0.258 ± 0.008	6.924 ± 0.001	0.384 ± 0.006	9.36 ± 0.04	0.4318 ± 0.008	7.01 ± 0.06	0.358 ± 0.009	8.99 ± 0.01	0.28 ± 0.01	11.23 ± 0.03	0.13 ± 0.01	7.29 ± 0.02
Na_2O	0.003 ± 0.004	0.29 ± 0.09	0.002 ± 0.008	0.055 ± 0.06	0.021 ± 0.06	6.8 ± 0.1	0.003 ± 0.008	0.06 ± 0.01	0.04 ± 0.03	5.92 ± 0.02	0.006 ± 0.008	0.28 ± 0.02	0.002 ± 0.003	0.020 ± 0.008
K_2O		11.2 ± 0.2		5.97 ± 0.09		0.048 ± 0.06		10.33 ± 0.09		0.036 ± 0.005		0.13 ± 0.01		0.042 ± 0.005
Total	99.93	98.73	100.22	98.85	100.49	99.95	99.82	99.59	99.72	99.91	100.36	99.09	99.88	99.35
Fe^{3+}/Fe^c		0.75 ± 0.02[d]		0.81 ± 0.02[d]		0.889 ± 0.08		0.75 ± 0.02		0.886 ± 0.008		0.76 ± 0.01[d]		0.761 ± 0.008[d]
NBO/T		0.54 ± 0.07		0.67 ± 0.06		0.74 ± 0.06		0.53 ± 0.03		0.86 ± 0.02		0.78 ± 0.03		0.71 ± 0.01
$K_{Ca}^{ol\text{-}liq}$		0.065 ± 0.03		0.037 ± 0.01		0.039 ± 0.01		0.061 ± 0.01		0.039 ± 0.001		0.024 ± 0.001		0.018 ± 0.001
$K_{Mn}^{ol\text{-}liq}$		1.22 ± 0.04		0.96 ± 0.02		0.80 ± 0.01		1.38 ± 0.02		0.70 ± 0.02		0.669 ± 0.008		0.611 ± 0.008
$K_{D(Ca\text{-}Mn)}^{ol\text{-}liq}$		0.0535 ± 0.003		0.038 ± 0.01		0.05 ± 0.01		0.044 ± 0.01		0.055 ± 0.02		0.036 ± 0.001		0.030 ± 0.002

Run no.	EVD10		EVD11		EVD12		EVD13		EVD14		EVD15		EVD16	
Sample	FAQ1MC		FNQMC		FLQ1MC		FNQMC		FDAQMC		FDMC		FNQMC	
Temp. (°C)	1350		1380		1350		1380		1375		1375		1500	
$-\log f_{O2}$	0.6		0.68		0.68		0.68		0.68		0.68		0.68	
Time (min)	1045		1050		375		395		955		995		155	
	Olivine (15)	Glass (3)	Olivine (15)	Glass (3)	Olivine (15)	Glass (3)	Olivine (15)	Glass (3)	Olivine (15)	Glass (3)	Olivine (15)	Glass (3)	Olivine (15)	Glass (3)
SiO_2	41.5 ± 0.2	54.71 ± 0.02	41.8 ± 0.3	46.8 ± 0.1	42.1 ± 0.6	56.0 ± 0.1	41.9 ± 0.2	46.8 ± 0.1	41.9 ± 0.1	50.2 ± 0.3	41.9 ± 0.2	49.8 ± 0.1	42.1 ± 0.2	46.0 ± 0.4
Al_2O_3		11.80 ± 0.01		11.2 ± 0.1		12.03 ± 0.06		11.22 ± 0.07		7.41 ± 0.06		0.015 ± 0.004		9.75 ± 0.05
FeO	0.96 ± 0.02	3.81 ± 0.04	1.6 ± 0.2	9.03 ± 0.01	0.985 ± 0.006	3.74 ± 0.04	1.77 ± 0.04	8.84 ± 0.6	2.26 ± 0.05	9.87 ± 0.06	2.02 ± 0.05	10.13 ± 0.06	1.53 ± 0.04	8.1 ± 0.1
MnO	1.45 ± 0.02	1.017 ± 0.006	0.76 ± 0.05	1.05 ± 0.02	1.42 ± 0.02	0.99 ± 0.02	0.791 ± 0.009	1.1 ± 0.1	0.78 ± 0.01	1.14 ± 0.02	0.81 ± 0.01	1.183 ± 0.007	0.669 ± 0.001	1.097 ± 0.004
MgO	55.2 ± 0.2	8.94 ± 0.07	55.7 ± 0.5	16.47 ± 0.03	54.5 ± 0.7	8.95 ± 0.04	55.4 ± 0.8	16.51 ± 0.06	55.1 ± 0.1	18.2 ± 0.1	54.4 ± 0.3	19.5 ± 0.3	55.6 ± 0.4	21.0 ± 0.2
CaO	0.49 ± 0.1	7.68 ± 0.02	0.37 ± 0.03	8.90 ± 0.01	0.54 ± 0.07	7.44 ± 0.02	0.37 ± 0.06	8.75 ± 0.08	0.283 ± 0.008	12.69 ± 0.09	0.67 ± 0.02	18.7 ± 0.2	0.35 ± 0.01	8.1 ± 0.3
Na_2O	0.002 ± 0.003	0.06 ± 0.06	0.028 ± 0.001	6.28 ± 0.02	0.004 ± 0.003	0.064 ± 0.001	0.04 ± 0.06	6.55 ± 0.09	0.002 ± 0.003	0.004 ± 0.005	0.002 ± 0.004	0.045 ± 0.004	0.021 ± 0.007	5.5 ± 0.3
K_2O		10.38 ± 0.07		0.043 ± 0.001		10.54 ± 0.009		0.043 ± 0.004		0.024 ± 0.004		0.048 ± 0.004		0.030 ± 0.006
Total	99.59	98.40	100.30	99.80	99.55	99.77	100.26	99.85	100.30	99.59	99.82	99.44	100.23	99.66
Fe^{3+}/Fe^c		0.75 ± 0.02		0.886 ± 0.008		0.75 ± 0.02		0.886 ± 0.008		0.813 ± 0.007[d]		0.81 ± 0.02[d]		0.874 ± 0.008
NBO/T		0.58 ± 0.01		0.86 ± 0.03		0.56 ± 0.03		0.87 ± 0.02		0.98 ± 0.02		1.59 ± 0.05		1.12 ± 0.06
$K_{Ca}^{ol\text{-}liq}$		0.062 ± 0.002		0.040 ± 0.003		0.07 ± 0.01		0.041 ± 0.006		0.022 ± 0.001		0.034 ± 0.001		0.041 ± 0.002
$K_{Mn}^{ol\text{-}liq}$		1.38 ± 0.02		0.69 ± 0.05		1.41 ± 0.03		0.72 ± 0.02		0.66 ± 0.02		0.642 ± 0.009		0.585 ± 0.009
$K_{D(Ca\text{-}Mn)}^{ol\text{-}liq}$		0.045 ± 0001		0.058 ± 0.006		0.051 ± 0.007		0.056 ± 0.009		0.033 ± 0.001		0.053 ± 0.002		0.070 ± 0.003

Run no.	EVD18		EVD19		EVD20		EVD21		EVD22		EVD23		EVD26	
Sample	FDAQMC		FDMC		FDAkMC		FDAkMC		FAQ2MC		FDMC		FNQMC	
Temp. (°C)	1500		1500		1500		1375		1360		1375		1450	
$-\log f_{O2}$	0.68		0.68		0.68		0.68		0.68		0.68		0.68	
Time (min)	255		175		865		1145		3980		3980		1265	
	Olivine (15)	Glass (3)	Olivine (15)	Glass (3)	Olivine (15)	Glass (3)	Olivine (15)	Glass (3)	Olivine (15)	Glass (3)	Olivine (15)	Glass (3)	Olivine (15)	Glass (3)
SiO_2	42.1 ± 0.2	48.50 ± 0.04	42.0 ± 0.2	48.8 ± 0.4	41.8 ± 0.2	45.5 ± 0.2	41.7 ± 0.2	46.05 ± 0.03	41.8 ± 0.2	50.0 ± 0.1	42.1 ± 0.2	49.73 ± 0.06	41.7 ± 0.2	46.8 ± 0.3
Al_2O_3		5.82 ± 0.01		0.013 ± 0.06		0.013 ± 0.005				12.91 ± 0.06		0.026 ± 0.002		10.01 ± 0.07
FeO	2.02 ± 0.05	8.2 ± 0.2	1.78 ± 0.06	8.61 ± 0.07	0.68 ± 0.03	4.27 ± 0.07	0.74 ± 0.03	5.0 ± 0.1	2.3 ± 0.2	9.1 ± 0.1	1.97 ± 0.04	9.8 ± 0.2	1.74 ± 0.03	7.91 ± 0.06
MnO	0.601 ± 0.009	1.084 ± 0.008	0.66 ± 0.01	1.141 ± 0.004	0.614 ± 0.008	0.997 ± 0.006	0.76 ± 0.01	1.04 ± 0.02	0.69 ± 0.02	1.11 ± 0.02	0.749 ± 0.008	1.17 ± 0.02	0.682 ± 0.008	1.047 ± 0.006
MgO	54.9 ± 0.3	25.94 ± 0.01	54.7 ± 0.3	26.0 ± 0.5	54.7 ± 0.3	23.72 ± 0.01	54.12 ± 0.2	18.31 ± 0.02	54.6 ± 0.2	19.2 ± 0.2	54.5 ± 0.3	20.05 ± 0.03	55.5 ± 0.3	21.51 ± 0.05
CaO	0.33 ± 0.01	10.2 ± 0.2	0.67 ± 0.02	15.37 ± 0.09	1.92 ± 0.02	25.50 ± 0.06	2.33 ± 0.01	29.28 ± 0.07	0.115 ± 0.006	7.27 ± 0.03	0.69 ± 0.02	18.54 ± 0.04	0.311 ± 0.005	7.93 ± 0.03
Na_2O	0.001 ± 0.002	0.002 ± 0.002	0.002 ± 0.004	0.012 ± 0.004	0.006 ± 0.006	0.028 ± 0.004	0.005 ± 0.008	0.03 ± 0.01	0.006 ± 0.005	0.03 ± 0.02	0.01 ± 0.01	0.112 ± 0.006	0.021 ± 0.007	4.27 ± 0.05
K_2O		0.031 ± 0.009		0.047 ± 0.001		0.024 ± 0.004		0.02 ± 0.01		0.058 ± 0.004		0.049 ± 0.003		0.034 ± 0.005
Total	99.91	99.71	99.88	100.02	99.72	100.05	99.64	99.73	99.50	99.65	100.03	99.51	99.91	99.54
Fe^{3+}/Fe^{c}		0.794 ± 0.007		0.798 ± 0.007		0.79 ± 0.01		0.81 ± 0.01[d]		0.761 ± 0.008		0.817 ± 0.007		0.879 ± 0.008
NBO/T		1.42 ± 0.03		1.90 ± 0.09		2.54 ± 0.04		2.30 ± 0.02		0.73 ± 0.03		1.62 ± 0.03		1.08 ± 0.04
$K_{Ca}^{ol\text{-}liq}$		0.031 ± 0.001		0.042 ± 0.001		0.071 ± 0.001		0.074 ± 0.003		0.016 ± 0.001		0.035 ± 0.001		0.038 ± 0.001
$K_{Mn}^{ol\text{-}liq}$		0.54 ± 0.01		0.55 ± 0.01		0.579 ± 0.009		0.6 ± 0.1		0.62 ± 0.02		0.60 ± 0.01		0.632 ± 0.009
$K_{D(Ca\text{-}Mn)}^{ol\text{-}liq}$		0.0578 ± 0.003		0.075 ± 0.003		0.122 ± 0.002		0.110 ± 0.005		0.025 ± 0.002		0.058 ± 0.002		0.060 ± 0.001

Run no.	EVD27		EVD28		EVD29		EVD43		EVD44	
Sample	FNQMC		GDAkMc		FDAkMC		FLQ1M		FDAk.5MCC	
Temp. (°C)	1400		1400		1450		1350°C		1375	
$-\log f_{O2}$	0.68		0.68		0.68		0.68		0.68	
Time (min)	1435		4020		1390		1460		1405	
	Olivine (15)	Glass (3)	Olivine (15)	Glass (3)	Olivine (15)	Glass (3)	Olivine (15)	Glass (3)	Olivine (15)	Glass (3)
SiO_2	42.0 ± 0.4	46.73 ± 0.04	41.8 ± 0.3	45.61 ± 0.01	41.7 ± 0.2	45.3 ± 0.1	41.9 ± 0.4	56.5 ± 0.1	41.7 ± 0.3	48.9 ± 0.2
Al_2O_3		11.32 ± 0.04		0.021 ± 0.003		0.01 ± 0.04		12.99 ± 0.01		0.027 ± 0.005
FeO	1.74 ± 0.04	9.29 ± 0.06	0.75 ± 0.03	4.98 ± 0.01	0.74 ± 0.02	4.60 ± 0.09	0.80 ± 0.03	3.22 ± 0.02	1.29 ± 0.03	6.8 ± 0.2
MnO	0.77 ± 0.02	1.05 ± 0.01	0.73 ± 0.2	1.01 ± 0.01	0.65 ± 0.01	0.98 ± 0.04	1.223 ± 0.007	0.803 ± 0.008	0.753 ± 0.008	1.07 ± 0.01
MgO	55.7 ± 0.3	16.82 ± 0.04	54.6 ± 0.4	19.66 ± 0.08	54.5 ± 0.3	22.23 ± 0.04	55.7 ± 0.4	9.47 ± 0.01	55.5 ± 0.3	20.00 ± 0.05
CaO	0.33 ± 0.01	8.94 ± 0.09	2.22 ± 0.03	28.3 ± 0.02	2.08 ± 0.04	26.31 ± 0.04	0.41 ± 0.02	6.10 ± 0.02	1.15 ± 0.03	23.5 ± 0.2
Na_2O	0.024 ± 0.05	5.14 ± 0.09	0.002 ± 0.003	0.06 ± 0.01	0.001 ± 0.001	0.031 ± 0.007	0.001 ± 0.001	0.047 ± 0.001	0.002 ± 0.003	0.03 ± 0.02
K_2O		0.029 ± 0.004		0.030 ± 0.004		0.031 ± 0.007		11.45 ± 0.03		0.026 ± 0.006
Total	100.59	99.31	100.09	99.63	99.71	99.43	100.07	100.56	100.38	100.39
Fe^{3+}/Fe^{c}		0.884 ± 0.008		0.81 ± 0.01		0.80 ± 0.01		0.75 ± 0.02		0.82 ± 0.01
NBO/T		0.83 ± 0.02		2.36 ± 0.03		2.48 ± 0.04		0.53 ± 0.02		2.24 ± 0.04
$K_{Ca}^{ol\text{-}liq}$		0.036 ± 0.01		0.073 ± 0.001		0.073 ± 0.001		0.067 ± 0.003		0.049 ± 0.001
$K_{Mn}^{ol\text{-}liq}$		0.71 ± 0.02		0.67 ± 0.02		0.629 ± 0.003		1.51 ± 0.03		0.70 ± 0.01
$K_{D(Ca\text{-}Mn)}^{ol\text{-}liq}$		0.051 ± 0.002		0.108 ± 0.003		0.119 ± 0.006		0.045 ± 0.002		0.070 ± 0.002

[a] These starting compositions are those for which Na and K serve only to charge-compensate Al^{3+} in tetrahedral coordination in melt and only Ca, Mg, and Fe^{2+} are network-modifying cations (see also text for more detailed discussion of these melts).

[b] Number in parentheses denotes number of analyses in average.

[c] $Fe^{3+}/\Sigma Fe$ calculated as described in text.

[d] $Fe^{3+}/\Sigma Fe$ determined by Mossbauer analysis.

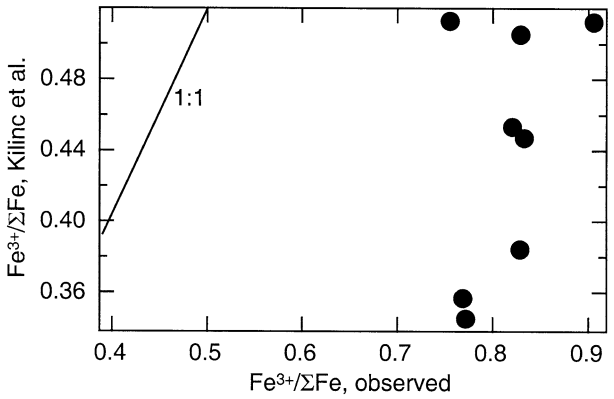

Fig. 6. Comparison of $Fe^{3+}/\Sigma Fe$ of glass formed by quenching of melt in equilibrium with olivine in air at 1350–1400°C obtained by Mössbauer spectroscopy ($Fe^{3+}/\Sigma Fe$ observed) and calculated with the empirical algorithm of Kilinc et al. (1983) ($Fe^{3+}/\Sigma Fe$).

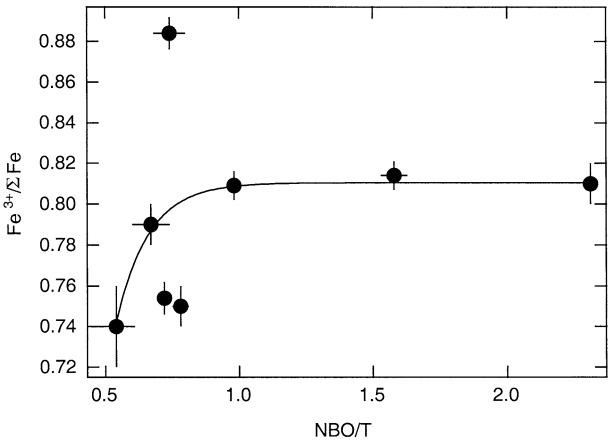

Fig. 7. Comparison of $Fe^{3+}/\Sigma Fe$ of glass formed by quenching of melt in equilibrium with olivine in air at 1350–1400°C obtained by Mössbauer spectroscopy as function of NBO/T of the melt. The 3 data points that do not fall on the simple exponential fit to the data in this figure probably reflect the fact that $Fe^{3+}/\Sigma Fe$ in silicate melts not only depends on NBO/T, but also on additional composition parameters such as Si/Al and the type and proportions of alkali and alkaline earths in the melt (see Mysen, 1995, for review).

Kilinc et al. (1983) empirical relationship between $Fe^{3+}/\Sigma Fe$, f_{O2}, temperature, and melt composition.

An alternative approach to estimate $Fe^{3+}/\Sigma Fe$ of the those melts for which $Fe^{3+}/\Sigma Fe$ was not determined is to use relationships between $Fe^{3+}/\Sigma Fe$ and melt composition from the samples for which $Fe^{3+}/\Sigma Fe$ was determined (Fig. 7). The exponential function fitted to these data was used to estimate the $Fe^{3+}/\Sigma Fe$ of unknowns in the 1350–1400°C temperature range. For melts outside this temperature range, the relationships between log (Fe^{3+}/Fe^{2+}) and 1/T reported by Mysen et al. (1985) for melts in the system Na_2O-CaO-MgO-Al_2O_3-SiO_2-Fe-O at ambient pressure were employed. This system is suitable for this purpose because most of the melts in the present study are also within this system. There are two K_2O-bearing starting materials, FLQ1MC and FLQ2MC. Existing data on redox equilibria of iron do not address temperature effects for K-bearing melt compositions. However, as compositions FLQ1MC and FLQ2MC were not used to examine temperature effects on olivine/melt partition coefficients, this is not a problem in the present study.

From the experimental data on redox relations of iron in melts in the Na_2O-CaO-MgO-Al_2O_3-SiO_2-Fe-O system (Mysen et al., 1985), the average free energy of reduction of Fe^{3+} to Fe^{2+}, ΔG, was 24 kJ/mol. This ΔG is slightly and positively correlated with the ionization potential of the metal cation, Al/(Al + Si), and NBO/T of the melt. These latter effects are relatively small, however, and for the purpose of extrapolation of temperature effects on Fe^{3+}/Fe^{2+} to the present system, the results in Mysen et al. (1985) do not provide a sufficiently wide compositional range to quantify these relationships in detail. The uncertainty in ΔG introduced by this lack of detailed knowledge appears to be around 25%. A 25% uncertainty in ΔG translates to ~7% relative uncertainty in $Fe^{3+}/\Sigma Fe$ for the present samples. This uncertainty, in turn, translates to an uncertainty of ≤1.2% (relative) in NBO/T-values. The uncertainties in the NBO/T-values of melts for which $Fe^{3+}/\Sigma Fe$ was calculated with this method include a ~1% relative uncertainty in the calculated $Fe^{3+}/\Sigma Fe$ values.

3.2. Olivine-Melt Partitioning Behavior

Experimental results from the 9 base compositions (the first 9 compositions in Table 1) conducted at the f_{O2} of air ($10^{-0.68}$) are summarized in Table 3. In these samples, the MnO and CaO contents of olivine are so low (Table 3) that variations in partition coefficients with composition likely reflect the structural behavior of Ca and Mn in the melt. This conclusion is substantiated by experimental results in the system CaO-MgO-MnO-Al_2O_3-SiO_2 (Watson, 1977; Jurewicz and Watson, 1988). These latter data indicate that the $K_{Ca}^{olivine-melt}$ and $K_{Mn}^{olivine-melt}$ (=$CaO^{olivine}/CaO^{melt}$ and $MnO^{olivine}/MnO^{melt}$, respectively) appear independent of CaO and MnO concentration in the olivine in CaO and MnO concentration ranges similar to those in the olivine studied here. That conclusion is consistent with composition-activity relations in Ca- and Mn-bearing forsterite in the MnO and CaO concentration relevant to the present study (Schwerdtfeger and Muan, 1966; Warner and Luth, 1974).

Olivine-melt partition coefficients for Ca and Mn, $K_{Ca}^{olivine/melt}$ and $K_{Mn}^{olivine/melt}$, are shown as a function of NBO/T at 1350–1400°C in Figure 8A, B. These data compare well with those of Jurewicz and Watson (1988) and Colson et al. (1988) for $K_{Ca}^{olivine/melt}$ and Watson (1977) and Colson et al. (1988) for $K_{Mn}^{olivine/melt}$. The $K_{Mn}^{olivine/melt}$ data of Colson et al. (1988) were from experiments with log $f_{O2} < -10$, which would be consistent with all Mn being in the divalent state in their melts. The data from Watson (1977) as well as the present data were obtained for experiments in air. That difference in f_{O2} notwithstanding, all the $K_{Mn}^{olivine/melt}$ data are in good agreement (Fig. 8B). For completeness, $K_{Fe^{2+}}^{olivine/melt}$ and $K_{Mg}^{olivine/melt}$ are also shown in Figure 8C, D and compared with the results of Kushiro and Mysen (2002), Colson et al. (1988) ($K_{Fe^{2+}}^{olivine/melt}$ and $K_{Mg}^{olivine/melt}$), and Jurewicz and Watson (1988) ($K_{Mg}^{olivine/melt}$). The agreement between the data is good.

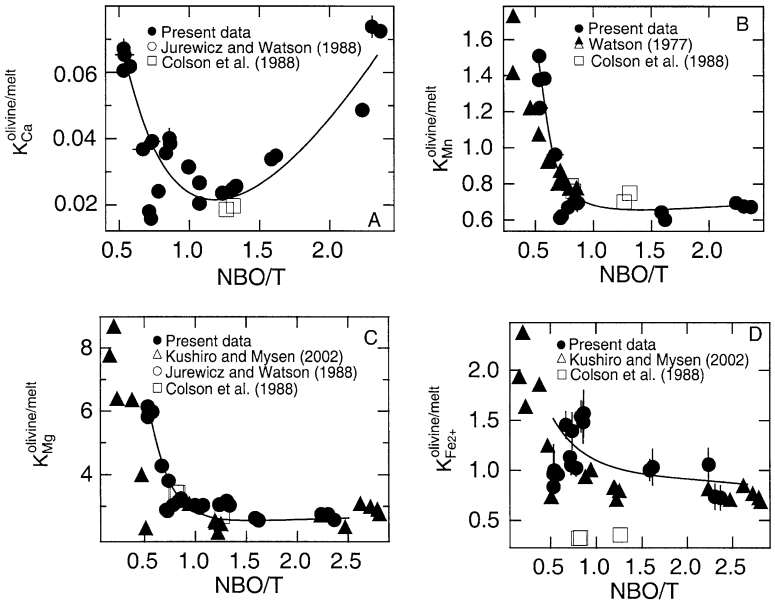

Fig. 8. Partition coefficients (wt% oxide in olivine/wt% oxide in melt) at 1350–1400°C at the f_{O2} of air as function of the NBO/T (data in Table 3) of the melt for Ca (A-$K_{Ca}^{olivine/melt}$), Mn (B-$K_{Mn}^{olivine/melt}$), Mg (C-$K_{Mg}^{olivine/melt}$), and Fe^{2+} (D-$K_{Fe^{2+}}^{olivine/melt}$) compared with existing data as indicated on diagrams. Published data are within the same temperature range as the present data. The data shown are for run durations of 995 min and longer (more than that needed to reach equilibrium; see Fig. 2 and discussion in text). The data for higher temperatures than 1350–1400°C are not shown because of possible temperature effects on olivine/melt partitioning might obscure composition-induced effects. Further, for reasons discussed in the text, data from experiments with Na/Ca are not included in this figure, but are presented and discussed separately (Fig. 13).

Both $K_{Ca}^{olivine/melt}$ and $K_{Mn}^{olivine/melt}$ decrease rapidly with increasing NBO/T with minimum K-values at NBO/T near 1. Similar behavior can be seen for $K_{Mg}^{olivine/melt}$ and to less accurate degree for $K_{Fe^{2+}}^{olivine/melt}$.

The relationship between $K_{Ca}^{olivine/melt}$ and $K_{Mn}^{olivine/melt}$ and the NBO/T of the melt is distinctly nonlinear. With NBO/T <1, both K-values decrease with increasing NBO/T of the melt. For NBO/T values above ~ 1, the $K_{Ca}^{olivine/melt}$ increases, whereas the partition coefficients for Mn, Mg, and Fe^{2+} appear nearly independent of NBO/T.

Interestingly, $K_{Ca}^{olivine/melt}$ generally is positively correlated with the Fo content of olivine at least from experiments in the 1350–1400°C temperature range (Fig. 9A) This relationship could be the result of mixing behavior in the olivine or because of melt structural control on Fe^{2+}-Mg exchange between the olivine and the melt. The latter explanation is the most likely because (i) the Fo content of the olivine in equilibrium with melt also exhibits a parabolic pattern with a minimum Fo value at NBO/T of the melt near 1 (Fig. 9B). In fact, this relationship resembles the shape of the $K_{Ca}^{olivine/melt}$ vs. NBO/T (Fig. 9A). Given those relations, it is not surprising that $K_{Ca}^{olivine/melt}$ is positively correlated with mol% Fo. (ii) The mixing data for olivine of the type under consideration here are not consistent with deviations from Henrian or Raoultian behavior (Schwerdtfeger and Muan, 1966; Warner and Luth, 1974; Watson, 1977; Watson and Jurewicz, 1988). (iii) Finally, the positive correlation between $K_{Ca}^{olivine/melt}$ and mol% Fo does not hold for the low f_{O2} experiments where the Fo content of the olivine is much lower than in the other experiments. Further, the database of Colson et al. (1988), where the olivine was

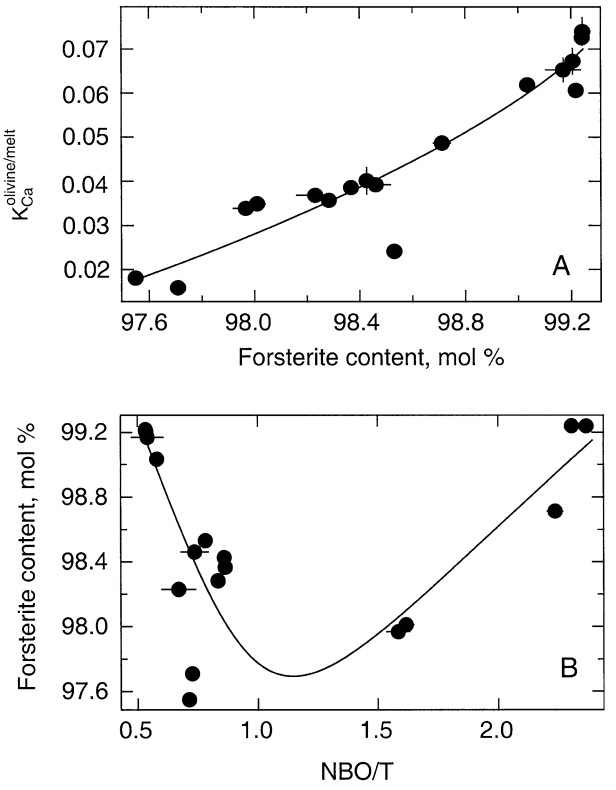

Fig. 9. (A) Partition coefficients (wt% oxide in olivine/wt% oxide in melt) at 1350–1400°C at the f_{O2} of air as function of forsterite content of olivine. B. Forsterite content of olivine as a function of NBO/T of coexisting melt at 1350–1400°C at the f_{O2} of air (data from Table 3).

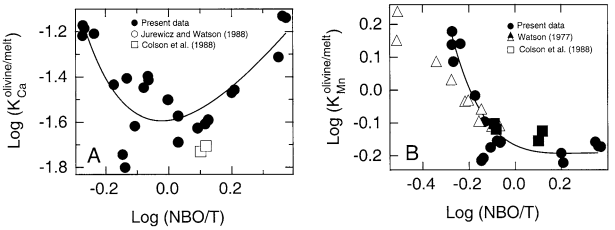

Fig. 10. Log-log relationships between NBO/T of the melt and $K_{Ca}^{olivine/melt}$ (A) and $K_{Mn}^{olivine/melt}$ (B) at 1350–1400°C at the f_{O2} of air (data from Table 3). Least squares regression of partition coefficients versus NBO/T for NBO/T <1 yields: Log $K_{Ca}^{olivine/melt}$ = −2.3 ± 0.7–1.8 ± 0.1Log(NBO/T), and Log $K_{Mn}^{olivine/melt}$ = −0.87 ± 0.12–0.22 ± 0.03Log(NBO/T). The data shown are for run durations of 995 min and longer (more than that needed to reach equilibrium; see Fig. 2 and discussion in text). The data for higher temperatures than 1350–1400°C are not shown because of possible temperature effects on olivine/melt partitioning might obscure composition-induced effects. Further, for reasons discussed in the text, data from experiments with Na/Ca are not included in this figure, but are presented and discussed separately (Fig. 13).

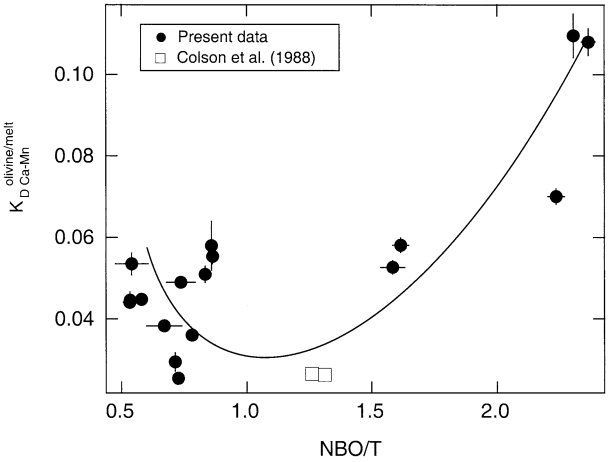

Fig. 11. Exchange equilibrium coefficient, $K_{D\ Ca-Mn}^{olivine/melt}$ [=CaO(olivine)/CaO(melt)/MnO(olivine)/MnO(melt)] at 1350–1400°C at the f_{O2} of air as function of the NBO/T of the melt (data from Table 3). See text for discussion of the data from Colson et al. (1988). The data shown are for run durations of 995 min and longer (more than that needed to reach equilibrium; see Fig. 2 and discussion in text). The data for higher temperatures than 1350–1400°C are not shown because of possible temperature effects on olivine/melt partitioning might obscure composition-induced effects. Further, for reasons discussed in the text, data from experiments with Na/Ca are not included in this figure, but are presented and discussed separately (Fig. 13).

also much more iron-rich, there is not evidence for relationships between Fo composition and $K_{D\ Ca}$.

In an experimental study of clinopyroxene-melt partitioning of Co, Ni, Mn, Mg, and Fe^{2+} at 1068°C. Toplis and Corgne (2002) suggested that relationships between $K_{M^{2+}}^{mineral-melt}$ and NBO/T of the melt can be described with a general expression of the form:

$$\text{Log } K_{M2+}^{mineral/melt} = -0.58 \log (\text{NBO/T}) + C. \quad (1)$$

In Eqn. 1, C is a constant whose value was assumed to depend on the mineral in question (Toplis and Corgne, 2002).

The NBO/T-range for which the relationship in Eqn. 1 was calibrated was 0.1–0.7. The NBO/T-range of the present study was wider (~0.5–2.5). In this wider NBO/T interval, the log $K_{Ca}^{olivine/melt}$ and log $K_{Mn}^{olivine/melt}$ versus log (NBO/T) are both distinctly nonlinear (Fig. 10). Straight-line relationships are, however, consistent with these data for NBO/T <1 and, thus, in principle accord with the results of Toplis and Corgne (2002) although the slope of these relationships differs from −0.58 (see caption, Fig. 10). This latter difference may, however, be because of the several hundred °C higher temperatures of the present experimental results. The nonlinear relations for the wider NBO/T range of the present data may be because NBO/T is not the only melt structure parameter governing mineral/melt partitioning behavior.

3.3. Exchange Equilibria and Melt Composition

The relationships between partition coefficients and NBO/T in Figure 8 lead to the suggestion that the Ca and Mn might exhibit different structural behavior in the melt as also suggested from Fe^{2+}-Mg exchange equilibria between olivine and melt under similar conditions (Kushiro and Mysen, 2002). Exchange equilibria of pairs of cations between olivine and melt can be used to address relative stability of cation-oxygen polyhedra in melts if activity-composition relations in the olivine do not vary in the element concentration range of interest.

As discussed above, the Ca-Mn exchange equilibrium between olivine and melt meets this requirement.

For the exchange equilibrium,

$$Mn^{2+}(\text{olivine}) + Ca^{2+}(\text{melt}) \Leftrightarrow Mn^{2+}(\text{melt}) + Ca^{2+}(\text{olivine}). \quad (2)$$

The exchange equilibrium constant is:

$$K_D^{olivine/melt} = \frac{a_{Ca^{2+}(olivine)} \cdot a_{Mn^{2+}(melt)}}{a_{Ca^{2+}(melt)} \cdot a_{Mn^{2+}(olivine)}} \quad (3)$$

where $a_{Ca^{2+}(olivine)}$ etc. is the activity of Ca^{2+} in olivine etc. Substitution of activity coefficients, γ_i, and mol fraction, X_i, for activity yields:

$$K_D^{olivine/melt} = \frac{\gamma_{Ca^{2+}}(\text{olivine}) \cdot X_{Ca^{2+}}(\text{olivine}) \cdot \gamma_{Mn^{2+}}(\text{melt}) \cdot X_{Mn^{2+}}(\text{melt})}{\gamma_{Ca^{2+}}(\text{melt}) \cdot X_{Ca^{2+}}(\text{melt}) \cdot \gamma_{Mn^{2+}}(\text{olivine}) \cdot X_{Mn^{2+}}(\text{olivine})} \quad (3a)$$

The $K_{D\ Ca-Mn}^{olivine/melt}$ is defined as:

$$K_{D\ Ca-Mn}^{olivine/melt} = \frac{X_{Ca^{2+}}(\text{olivine}) \cdot X_{Mn^{2+}}(\text{melt})}{X_{Ca^{2+}}(\text{melt}) \cdot X_{Mn^{2+}}(\text{olivine})} \quad (4)$$

At constant temperature, $K_D^{olivine/melt}$ (Eqn. 3) is constant. Further, as discussed above, the activity coefficient ratio, $\gamma_{Ca^{2+}(olivine)}/\gamma_{Mn^{2+}(olivine)}$ is constant in the CaO and MnO concentration range in the olivine under study. It follows, therefore, that;

$$K_{D\ Ca-Mn}^{olivine/melt} = \text{const} \cdot \frac{\gamma_{Ca^{2+}}(\text{melt})}{\gamma_{Mn^{2+}}(\text{melt})} \quad (5)$$

The $K_{D\ Ca-Mn}^{olivine/melt}$ varies systematically with the NBO/T of the melt (Fig. 11). It decreases with increasing NBO/T from

NBO/T <1 until NBO/T~1. After a minimum at NBO/T~1, the $K_D^{olivine/melt}{}_{Ca\text{-}Mn}$ again increases. The two data points from Colson et al. (1988) at 1364°C fall near the line defining this relationship even though the olivine in those to experiments (Fo_{63} and Fo_{64}) was considerably more iron-rich than the olivine in the present study (Fo_{97}-$Fo_{99.5}$). From the data in Figure 11 and the relationship Eqn. 5 it follows, therefore, that the activity coefficient ratio in the melt, $\gamma_{Ca^{2+}}$(melt)/$\gamma_{Mn^{2+}}$(melt), passes through a minimum value for melts with NBO/T~1. In other words, the relative stability of Mn and Ca in silicate melts depends on the degree of polymerization of silicate melts.

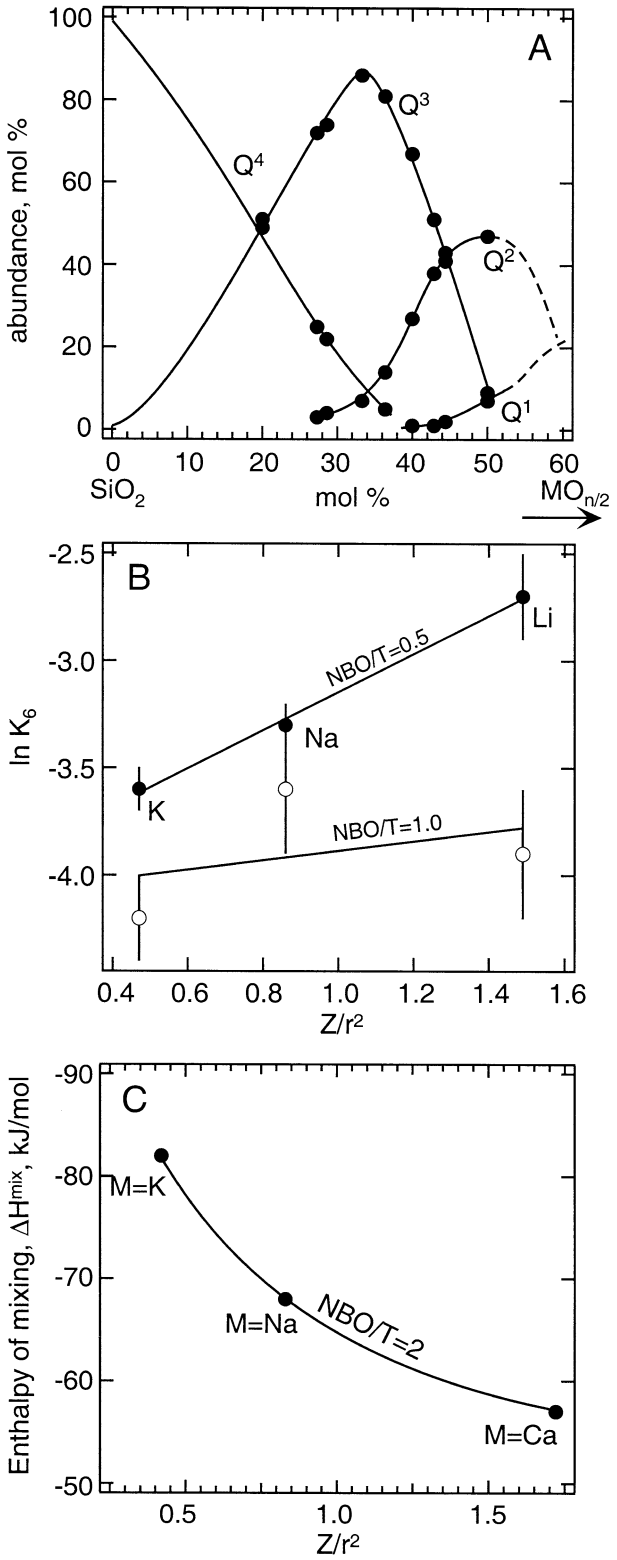

Fig. 12. Melt structure and properties along metal oxide-silica joins. (A) Abundance of structural units (Q^n-species) in glass along the join SiO_2-K_2O (M = K) as a function of melt composition (from Maekawa et al., 1991). Note that the topology of Q^n versus melt NBO/T relations is similar for all alkali and alkaline earth silicate melts (Mysen, 1990, 1995). (B) Equilibrium constant for the equilibrium, $2Q^3 \Leftrightarrow Q^2 + Q^4$ (n = 3 in Eqn. 6) for melts and supercooled melts in the systems Li_2O-SiO_2, Na_2O-SiO_2, and K_2O-SiO_2 at T ~ 1050°C and ambient pressure for melt compositions with NBO/T = 1 and 0.5 (T = Si in these melts) (from data summary in Mysen, 1995). (C) Enthalpy of mixing in melts along the joins $KO_{1/2}$-SiO_2, $NaO_{1/2}$-SiO_2, and CaO-SiO_2 for melts with NBO/T = 2 (T = Si) (data compilation by Navrotsky et al., 1985).

The relationships in Figure 11 probably reflect competition between Ca and Mn for nonbridging oxygen in the melt. These nonbridging oxygens have different properties depending on the Q^n-species that exist in the melts. The equilibrium between the Q^n-species can be expressed with the generalized expression (e.g., Stebbins, 1987):

$$2Q^n \Leftrightarrow Q^{n-1} + Q^{n+1} \quad (6)$$

where the Q^n-species are defined in terms of their number of bridging oxygen, n (nonbridging oxygen, NBO = 4-n) per tetrahedrally coordinated cation. The abundance of the individual Q^n-species is a systematic function of the melt composition in binary metal oxide-silica melts (Fig. 12A). For most rock-forming igneous melts their NBO/T-range is such that n = 3 and the dominant Q^n-species are Q^4, Q^3, and Q^2 (Mysen, 1988). The abundance of Q^3-species, regardless of metal cation properties, reaches a maximum in melts whose NBO/T-value is near 1 (for review of structure data, see Mysen, 1995).

The relative abundance of the Q^n-species depends not only on the NBO/T of the melt, but also on the ionization potential of the network-modifying metal cation (ionization potential, Z/r^2, where Z is the electrical charge and r is the ionic radius) (Mysen, 1995). For systems with n = 3, the equilibrium constant for equilibrium 6, ln K_6, is a simple and positive function of the ionization potential of the metal cation at constant temperature and NBO/T of the melt (Fig. 12B). This relationship does not, however, change the NBO/T-value of the melt at which the Q^3-abundance reaches a maximum (see Mysen, 1995).

The stability of metal cation-NBO bonds (NBO, nonbridging oxygen) in individual Q^n-species depends on the ionic radius and charge of the metal cation. In a Q^3-species, for example, there is 1 nonbridging oxygen per silicate tetrahedron. The negative electric charge associated with this nonbridging oxygen is neutralized via bonding to network-modifying cations. The smaller their ionic radius, or the greater their electrical charge, the less stable is the metal−NBO(Q^3) bond. Such structural effects have been documented via ^{17}O NMR spectroscopy of mixed alkali metal/alkaline earth silicate glasses (Jones et al., 2001; Lee et al., 2002; Lee and Stebbins, 2003).

These melt structural features probably also govern other melt properties such as, for example, enthalpy of mixing along binary metal oxide-silica joins (Fig. 12C, see also Navrotsky et al., 1985). These structural principles are also similar to those that govern relationships between the structure of simple silicate crystals and metal cation properties (see Liebau, 1981, for detailed review).

We suggest that the relationships between $K_{D\ Ca\text{-}Mn}^{olivine/melt}$ and the NBO/T of the melt exist because different relative stability of Ca-NBO and Mn-NBO bonds in Q^n-species in the melt is controlled by the ionic radius difference between Ca^{2+} and Mn^{2+} (~25%; Whittaker and Muntus, 1970). We suggest that Mn-NBO(Q^3) bonds are less stable than Ca-NBO(Q^3) bonds because $Z/r^2(Mn) > Z/r^2(Ca)$. Therefore, $\gamma_{Ca^{2+}(melt)}/\gamma_{Mn^{2+}(melt)}$ is likely to decrease as the Q^3-abundance of the melt, which is controlled by its major element composition, increases. The Q^3-abundance reaches its maximum at NBO/T~1, which is, therefore, where $\gamma_{Ca^{2+}(melt)}/\gamma_{Mn^{2+}(melt)}$ attains a minimal value. The Q^3-abundance decreases on either side of this NBO/T~1-value. With NBO/T <1, this is likely to cause primarily an increase in the $\gamma_{Ca^{2+}}$(melt) and, thus, an increase in $\gamma_{Ca^{2+}(melt)}/\gamma_{Mn^{2+}(melt)}$. If Q^n-species less polymerized than Q^3 are available (as is the case in melts with NBO/T >1), Mn^{2+} likely would tend to form Mn-NBO bonds (NBO-nonbridging oxygen) in such species (Q^2, Q^1, and Q^0) thus possibly leading to a decrease in $\gamma_{Mn^{2+}}$(melt), and, thus, and increase in $\gamma_{Ca^{2+}(melt)}/\gamma_{Mn^{2+}(melt)}$.

Additional partitioning data relevant to possible melt structural control of mineral/melt partitioning may be found by examination of relationships between the Ca⇔Mn exchange equilibrium constant and melts whose structure is affected by exchange of some of the Ca^{2+} with Na^+. The $Ca^{2+}⇔Na^+$ exchange is of interest because of the similar ionic radius but different ionic charge of these two cations (their ionization potentials do, therefore, differ substantially—$Z/r^2(Ca)$~$2Z/r^2(Na)$). One may expect, therefore, the abundance of nonbridging oxygen in Q^3-species available for Ca-NBO(Q^3) bonds to decrease as Na/(Na + Ca) increases. Relationships between Na/(Na + Ca) and $K_{D\ Ca\text{-}Mn}^{olivine/melt}$ for three compositions with different NBO/T-values of the melt were examined (Table 4, Fig. 13). These melts were in equilibrium with olivine from starting compositions FNQMC, FDQMC, and FDAkMC. The 3 compositions were chosen for this purpose (a) because the large difference in NBO/T-values (~1, ~1.5, and ~2.3, respectively) implies significant differences in type and abundance of Q^n-species (e.g., Virgo et al., 1980; Schramm et al., 1984; Maekawa et al., 1991; Mysen and Frantz, 1994), and (b) because they contain no Al^{3+}. The presence of Al^{3+} would complicate this analysis because in aluminosilicate melts, portions of alkali metals and alkaline earths not only may be network-modifiers, but can also serve to charge-balance Al^{3+} in tetrahedral coordination in the melt (Mysen, 1997). The relative stability of tetrahedrally coordinated, charge-balanced Al^{3+} depends on the electronic properties of the cation(s) involved in this charge-balance. The order of stability is K > Na > Ca > Mg (Navrotsky et al., 1985).

Also shown in Figure 13 is the variation in NBO/T-value of the individual melts as a function of Na/(Na + Ca). These NBO/T-values vary because changes in Na/(Na + Ca) affect the relative proportions of olivine and melt even at the same temperature. For the FNQMC and FDMC starting compositions, the NBO/T-variation is ~10%, which has insignificant influence on the $K_{D\ Ca\text{-}Mn}^{olivine/melt}$-values in the NBO/T-range of these two melt compositions (Fig. 11). The NBO/T of melt from starting composition FDAkMC initially increases by ~10%, followed by an NBO/T-decrease of ~30% as Na/(Na + Ca) is increased further. From the data in Figure 11, this NBO/T-decrease, by itself, should result in a small decrease (maximum change = 15–20%) in $K_{D\ Ca\text{-}Mn}^{olivine/melt}$. These uncertainties notwithstanding, the $K_{D\ Ca\text{-}Mn}^{olivine/melt}$ is positively correlated with Na/(Na + Ca) of the melt. The rate of change of $K_{D\ Ca\text{-}Mn}^{olivine/melt}$ with increasing Na/(Na + Ca) decreases with increasing NBO/T-value of the melt. In other words, from Eqn. 5 the activity coefficient ratio, $\gamma_{Ca^{2+}(melt)}/\gamma_{Mn^{2+}(melt)}$, increases with increasing Na/(Na + Ca) of the melt. We suggest that this change reflects competition among Na^+ and Ca^{2+} for nonbridging oxygen in Q^3-species in the melts.

3.4. Exchange Equilibria and Temperature

The melt composition-dependent solubility behavior of Ca^{2+} and Mn^{2+} also is reflected in the enthalpy of reaction (2). From the temperature-dependence of $K_{D\ Ca\text{-}Mn}^{olivine/melt}$,

$$K_{D\ Ca\text{-}Mn}^{olivine/melt} = -(\Delta H/RT - \Delta S/R), \quad (7)$$

where ΔH and ΔS are the enthalpy and entropy change for equilibrium 2, T is the temperature (K) and R the gas constant. The slope of ln $K_{D\ Ca\text{-}Mn}^{olivine/melt}$ vs. 1/T (Fig. 14) defines ΔH provided that the change in NBO/T of the melt with temperature does not affect the $K_{D\ Ca\text{-}Mn}^{olivine/melt}$-values significantly. For composition FNQMC, where melts have NBO/T-values near the minimum in Figure 11, the NBO/T varies by ~30% in the 1350–1500°C temperature range (Fig. 14C). A 30% change in NBO/T near NBO/T = 1 does not, however, affect $K_{D\ Ca\text{-}Mn}^{olivine/melt}$ significantly (Fig. 11). For the other composition used for temperature studies, FDAkMC, the NBO/T of the melt increases from 2.3 to 2.55 between 1350° and 1500°C (Fig. 14D). At the temperature of the data in Figure 11 (1350–1400°C), such an increase in NBO/T results in an increase of $K_{D\ Ca\text{-}Mn}^{olivine/melt}$ from ~0.085 to ~0.11 (Fig. 11).

From the linear regression through the data in Figure 14, ΔH of equilibrium 2 for composition FNQMC is 55 ± 11 kJ/mol, whereas for composition FDAkMC the ΔH equals 33 ± 33 kJ/mol. Because the likely changes in $K_{D\ Ca\text{-}Mn}^{olivine/melt}$ with NBO/T resulting from the increase in temperature, the ΔH for composition FDAkMC is a maximum value. The larger ΔH-value for composition FNQMC compared with FDAkMC is consistent with the largest difference between γ_{Mn2+}(melt) and γ_{Ca2+}(melt) for melt composition whose NBO/T-value is near 1 (FNQMC).

3.5. Exchange Equilibria and Oxygen Fugacity

The observation that olivine/melt exchange equilibria such as that involving Ca and Mn depend on NBO/T and Qn species in the melt leads to the suggestion that any parameter that affects NBO/T may also affect the $K_{D\ Ca\text{-}Mn}^{olivine/melt}$. Variation in redox state of iron in silicate melts can causes changes in their NBO/T (Fig. 5C).

The redox ratio of iron in melt is governed by f_{O_2}. The $K_{D\ Ca\text{-}Mn}^{olivine/melt}$ as a function of log f_{O_2} for starting composition FDMC is shown in Figure 15 (Table 5). There is a small

Table 4. Chemical analyses of run products from starting compositions where Na/Ca ratio is main variable (wt%).

Run no.	EVD47		EVD48		EVD49		EVD50		EVD51		EVD52	
Sample	DMC-1		DMC-2		FDMC-3		FDAkMC-1		FDAkMC-2		FDAkMC-3	
Temp. (°C)	1375		1375		1375		1375		1375		1375	
$-\log f_{O_2}$	0.68		0.68		0.68		0.68		0.68		0.68	
Time (min)	1325		1465		1440		1440		1435		1445	
	Olivine (15)[a]	Glass (3)	Olivine (15)	Glass (3)	Olivine (15)	Glass (3)	Olivine (15)	Glass (3)	Olivine (15)	Glass (3)	Olivine (15)	Glass (3)
SiO_2	41.8 ± 0.2	51.69 ± 0.05	41.2 ± 0.3	51.3 ± 0.2	41.7 ± 0.2	54.2 ± 0.3	41.8 ± 0.2	47.9 ± 0.2	41.7 ± 0.3	49.14 ± 0.01	42.0 ± 0.3	52.59 ± 0.04
Al_2O_3		0.055 ± 0.005		0.034 ± 0.006		0.081 ± 0.008		0.022 ± 0.002		0.019 ± 0.008		0.018 ± 0.003
FeO	1.71 ± 0.04	10.14 ± 0.05	1.39 ± 0.05	10.5 ± 0.2	1.49 ± 0.05	10.1 ± 0.1	0.59 ± 0.03	5.02 ± 0.03	0.52 ± 0.03	5.00 ± 0.08	0.55 ± 0.08	5.76 ± 0.07
MnO	0.819 ± 0.008	1.087 ± 0.008	0.78 ± 0.01	1.06 ± 0.01	0.85 ± 0.01	1.043 ± 0.004	0.72 ± 0.01	0.988 ± 0.004	0.70 ± 0.02	1.003 ± 0.003	0.66 ± 0.06	1.067 ± 0.004
MgO	55.5 ± 0.2	18.89 ± 0.04	55.2 ± 0.3	19.3 ± 0.2	55.7 ± 0.2	18.8 ± 0.7	55.1 ± 0.3	19.53 ± 0.09	55.6 ± 0.3	19.9 ± 0.8	55.5 ± 0.8	20.09 ± 0.01
CaO	0.541 ± 0.007	12.83 ± 0.06	0.402 ± 0.009	8.1 ± 0.1	0.195 ± 0.008	3.43 ± 0.03	1.7 ± 0.1	21.7 ± 0.1	1.28 ± 0.02	16.15 ± 0.03	0.77 ± 0.02	11.5 ± 0.02
Na_2O	0.030 ± 0.008	5.08 ± 0.09	0.047 ± 0.005	9.8 ± 0.3	0.053 ± 0.008	12.51 ± 0.02	0.030 ± 0.007	4.98 ± 0.03	0.031 ± 0.06	9.06 ± 0.03	0.029 ± 0.009	10.84 ± 0.05
K_2O		0.256 (1)	0.031 (4)			0.041 ± 0.009		0.02 ± 0.01		0.06 ± 0.02		0.025 ± 0.009
Total	100.38	100.02	99.02	100.04	99.9	100.19	99.93	100.12	99.83	100.31	99.53	101.54
Fe^{3+}/Fe^b		0.81 ± 0.02		0.81 ± 0.02		0.81 ± 0.02		0.81 ± 0.01		0.81 ± 0.01		0.81 ± 0.01
NBO/T		1.71 ± 0.03		1.72 ± 0.05		1.47 ± 0.05		2.52 ± 0.02		2.37 ± 0.04		1.92 ± 0.01
$K_{Ca}^{ol\text{-}liq}$		0.042 ± 0.001		0.049 ± 0.001		0.056 ± 0.001		0.080 ± 0.005		0.078 ± 0.001		0.068 ± 0.02
$K_{Ma}^{ol\text{-}liq}$		0.746 ± 0.009		0.73 ± 0.01		0.81 ± 0.01		0.72 ± 0.01		0.69 ± 0.02		0.061 ± 0.05
$K_{D(Ca\text{-}Ma)}^{ol\text{-}liq}$		0.056 ± 0.01		0.068 ± 0.02		0.070 ± 0.002		0.110 ± 0.007		0.113 ± 0.004		0.11 ± 0.02

[a] Number in parentheses denotes number of analyses in average.
[b] Fe^{3+}/Fe calculated as described in text.

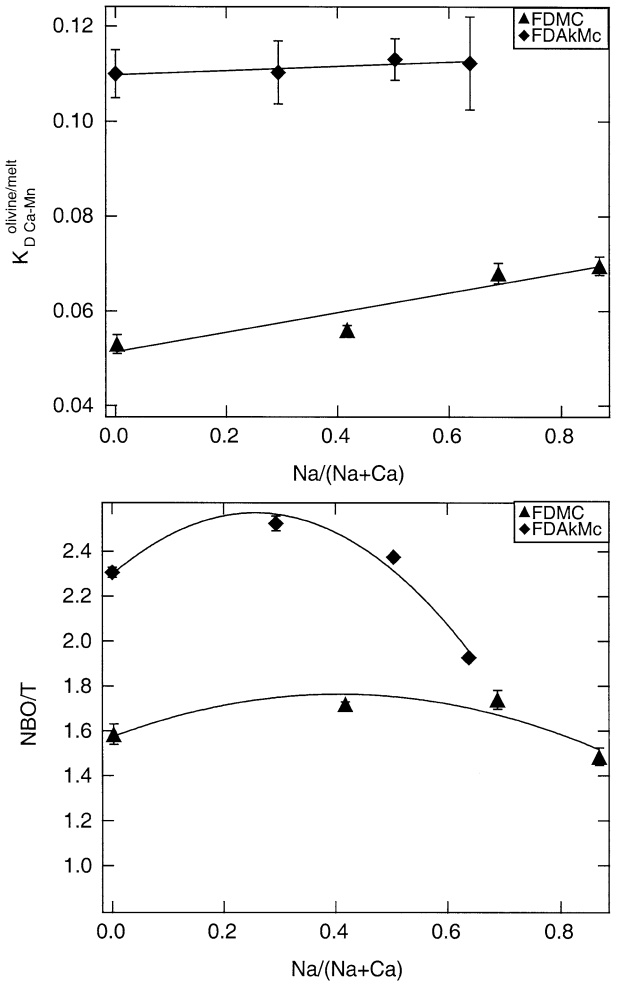

Fig. 13. Exchange equilibrium coefficient, $K_{D\ Ca\text{-}Mn}^{olivine/melt}$ [=CaO(olivine)/CaO(melt)/MnO(olivine)/MnO(melt)] as function of Na/(Na + Ca) of the melt and NBO/T of the melt as a function of Na/(Na + Ca), all at 1375°C, for starting compositions shown in the diagrams (data from Tables 3 and 4).

$K_{D\ Ca\text{-}Mn}^{olivine/melt}$ decrease with decreasing f_{O_2} and, therefore, with decreasing $Fe^{3+}/\Sigma Fe$ and increasing NBO/T (Fig. 5). Also shown in that figure (as dashed line) is the trend in $K_{D\ Ca\text{-}Mn}^{olivine/melt}$ versus NBO/T that would be expected if the Ca-Mn exchange partition coefficient varied simply as a function of the change in melt NBO/T (Fig. 11) controlled by the $Fe^{3+}/\Sigma Fe$ and oxygen coordination of Fe^{2+} and Fe^{3+} in the melt. An increase in $K_{D\ Ca\text{-}Mn}^{olivine/melt}$ expected from the $Fe^{3+}/\Sigma Fe$-driven change in NBO/T is not observed.

A possible explanation for the difference between those calculated and the actual $K_{D\ Ca\text{-}Mn}^{olivine/melt}$-values, expressed as a function of f_{O_2} in Figure 15, may be that Mn in the melt exists in more than one oxidation state. Alternatively, the activity-composition relations of Ca and Mn in the melt depend on oxygen fugacity.

In this latter case, because the concentration of CaO in the melts does not change significantly with oxygen fugacity (Tables 3 and 5), and neither CaO nor MnO concentration in olivine is sensitive to oxygen fugacity (Tables 3 and 5), the

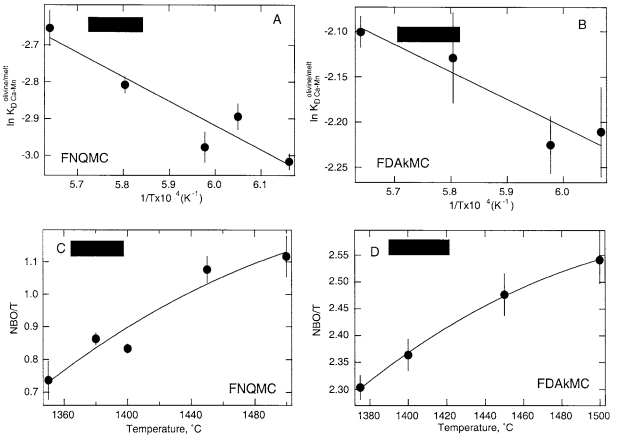

Fig. 14. Exchange equilibrium coefficient, $K_{D\ Ca\text{-}Mn}^{olivine/melt}$ [=CaO(olivine)/CaO(melt)/MnO(olivine)/MnO(melt)] of melts coexisting with olivine as a function of temperature (1350–1500°C) (data from Table 3). (A) $K_{D\ Ca\text{-}Mn}^{olivine/melt}$ as a function of temperature [1/T(K)] for starting composition FNQMC. (B) $K_{D\ Ca\text{-}Mn}^{olivine/melt}$ as a function of temperature [1/T(K)] for starting composition FDAkMC. (C) The NBO/T of melt coexisting with olivine as a function of temperature [1/T(K)] for starting composition FNQMC. (D) The NBO/T of melt coexisting with olivine as a function of temperature [1/T(K)] for starting composition FDAkMC.

activity coefficient ratio of Ca and Mn in the melt, $\gamma_{Ca^{2+}(melt)}/\gamma_{Mn^{2+}(melt)}$, decreases slightly (Eqn. 5) with decreasing oxygen fugacity (increasing NBO/T of the melt in equilibrium with olivine). However, from the relationship in Figure 11, increasing NBO/T of the melt actually results in an increase in $\gamma_{Ca^{2+}(melt)}/\gamma_{Mn^{2+}(melt)}$ because $K_{D\ Ca\text{-}Mn}^{olivine/melt}$ increases with NBO/T in the NBO/T-range under discussion. This is, therefore, an unlikely explanation for the relationships in Figure 15.

The more likely explanation is that Mn exists in multiple oxidation states in the melt, and that the Mn oxidation ratio depends on f_{O_2}. This is likely because in the crystalline state, the transformation of MnO to Mn_3O_4 at 1375°C occurs, for example, at $\log f_{O_2} = -2.2$ (Huebner, 1969). A portion of the Mn may, therefore, exist as Mn^{3+} in melts equilibrated with air ($\log f_{O_2} = -0.68$).

A general exchange equilibrium between olivine and melt where the oxidation state of Mn in the melt may be higher than 2+ (e.g., Mn^{3+}) in the olivine (Mn^{2+} is assumed for olivine) is:

$$CaO(melt) + MnO(olivine) + 1/4O_2 \Leftrightarrow MnO_{3/2}(melt) + CaO(olivine), \quad (8)$$

with the equilibrium constant (assuming activity equal to mol fraction):

$$K_8 = \frac{X_{CaO}(olivine)}{X_{CaO}(melt)} \cdot \frac{X_{MnO_{3/2}}(melt)}{X_{MnO}(olivine) \cdot (f_{O_2})^{1/4}}. \quad (8b)$$

If the oxidation state of Mn in olivine and melt was the same (2+), the exchange equilibrium is:

$$CaO(melt) + MnO(olivine) \Leftrightarrow CaO(olivine) + MnO(melt), \quad (9)$$

with the equilibrium constant:

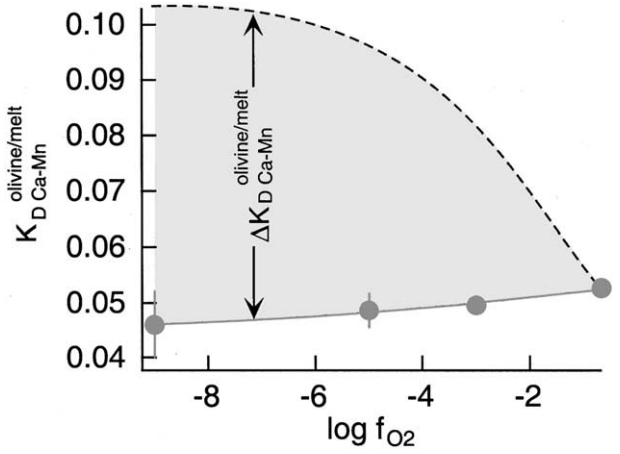

Fig. 15. Exchange equilibrium coefficient, $K_{D\ Ca\text{-}Mn}^{olivine/melt}$ [=CaO(olivine)/CaO(melt)/MnO(olivine)/MnO(melt)] as a function of oxygen fugacity (log f_{O_2}) at 1375°C for starting composition FDMC (data from Tables 3 and 5). Dashed line = estimated values of $K_{D\ Ca\text{-}Mn}^{olivine/melt}$ with NBO/T as discussed in text. $\Delta K_{D\ Ca\text{-}Mn}^{olivine/melt}$ is the difference between this calculated evolution of $K_{D\ Ca\text{-}Mn}^{olivine/melt}$ and the observed values.

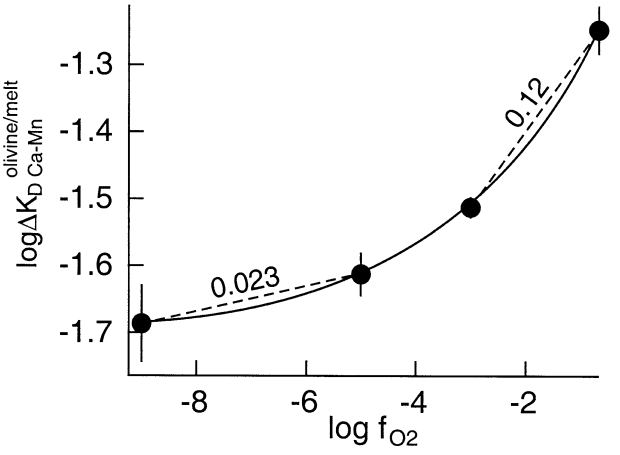

Fig. 16. Log $\Delta K_{D\ Ca\text{-}Mn}^{olivine/melt}$ (as defined in Eqn. 11) as a function of oxygen fugacity (log f_{O_2}). Dashed lines represent straight line connected between the two data points and number on line its slope (see text for detailed discussion).

$$K_9 = \frac{X_{CaO}(olivine)}{X_{CaO}(melt)} \cdot \frac{X_{MnO}(melt)}{X_{MnO}(olivine)} \qquad (9b)$$

The difference between K_8 and K_9, $\Delta K_{D\ Ca\text{-}Mn}^{olivine/melt}$, is:

$$\log \Delta K_{D\ Ca\text{-}Mn}^{olivine/melt} = \log K_8 - \log K_9, \qquad (10)$$

and, therefore:

$$\log \Delta K_{D\ Ca\text{-}Mn}^{olivine/melt} = \log\left(\frac{X_{Mn_2O_3}(melt)}{X_{MnO}(melt)}\right) - \frac{1}{4} \cdot \log f_{O_2}. \qquad (11)$$

Thus, the slope of the relationship between $\log \Delta K_{D\ Ca\text{-}Mn}^{olivine/melt}$ and log f_{O_2} reflects the oxidation state on Mn (see Fig. 16). The gradually decreasing value of log $\Delta K_{D\ Ca\text{-}Mn}^{olivine/melt}$ with decreasing f_{O_2} would then imply a gradual decrease of Mn^{3+}/Mn^{2+} in the melt under the assumption that the activity coefficient ratio, $\gamma_{Mn_2O_3}(melt)/\gamma_{MnO}(melt)$, remains constant. If this latter ratio equals unity, the slope can be used to determine the Mn^{3+}/Mn^{2+} in the melt.

The slope of the log $\Delta K_{D\ Ca\text{-}Mn}^{olivine/melt}$ versus log f_{O_2} in the f_{O_2}-range between that of air and 10^{-3} bar (where, for the equilibrium between MnO and Mn_2O_3, MnO would be stable; Huebner, 1969), is 0.12 (Fig. 16), which corresponds to $Mn^{2+}/(Mn^{2+} + Mn^{3+}) \sim 0.75$. We conclude, therefore, that even though there probably is a small fraction of Mn^{3+} in the melts coexisting with olivine in air, this ratio is low. That conclusion

Table 5. Chemical analyses of run products from experiments conducted with reduced oxygen fugacity (wt%).

Run no.	EVD56		EVD58		EVD59	
Sample	FDMC		FDMC		FDMC	
Temp. (°C)	1375		1375		1375	
−log f_{O_2}	3		5		9	
Time (min)	1335		1385		1410	
	Olivine (15)[a]	Glass (3)	Olivine (15)	Glass (3)	Olivine (15)	Glass (3)
SiO_2	41.0 ± 0.3	51.030 ± 0.1	41.6 ± 0.2	47.0 ± 0.4	41.2 ± 0.2	52.5 ± 0.2
Al_2O_3		0.020 ± 0.004		10.95 ± 0.01		0.030 ± 0.008
FeO	4.79 ± 0.05	9.66 ± 0.04	1.92 ± 0.05	8.37 ± 0.02	5.4 ± 0.6	7.02 ± 0.05
MnO	0.90 ± 0.01	1.108 ± 0.009	0.713 ± 0.009	0.933(8)	0.83 ± 0.04	1.055 ± 0.001
MgO	52.5 ± 0.5	18.2 ± 0.5	55.4 ± 0.2	17.94 ± 0.01	52.6 ± 0.5	19.02 ± 0.05
CaO	0.80 ± 0.01	19.7 ± 0.3	0.377 ± 0.009	13.79 ± 0.06	0.74 ± 0.09	20.34 ± 0.09
Na_2O	0.002 ± 0.003	0.013 ± 0.008	0.001 ± 0.001	0.022 ± 0.008	0.002 ± 0.004	0.047 ± 0.001
K_2O		0.044(1)		0.022(4)		0.034 ± 0.008
Total	99.99	99.75	100.02	99.05	100.76	100.08
$Fe^{3+}/Fe^{\#}$		0.43 ± 0.02		0.886 ± 0.008		0.0
NBO/T		2.14 ± 0.04		1.06 ± 0.05		2.36 ± 0.04
$K_{Ca}^{ol\text{-}liq}$		0.040 ± 0.01		0.027 ± 0.01		0.036 ± 0.04
$K_{Mn}^{ol\text{-}liq}$		0.81 ± 0.01		0.76 ± 0.01		0.78 ± 0.03
$K_{D(Ca\text{-}Mn)}^{ol\text{-}liq}$		0.050 ± 0.01		0.036 ± 0.01		0.046 ± 0.006

[a] Number in parentheses denotes number of analyses in average.

(only a small fraction of Mn more oxidized than Mn^{2+}) is consistent with the general agreement between the present olivine/melt Mn data and those of Colson et al. (1988), whose experiments were conducted at $-\log f_{O_2} = 10-11$ and where, therefore, all Mn is likely to be Mn^{2+} (e.g., Fig. 8). The agreement between these latter data and those of Watson (1977), also conducted in air, would suggest that in the latter experiments the proportion in the melt of Mn oxidation states above 2+ also was small.

4. CONCLUDING REMARKS

1. Partitioning of minor elements such as Ca and Mn between olivine and melt is sensitive to melt structure and reflects relative stabilities of Ca-O and Mn-O polyhedra associated with the structural units (Q^n-species) in the melt. Their relative stability probably is governed by differences in steric hindrance of Ca-NBO and Mn-NBO bonding in the different coexisting Q^n-species in the melt.

2. The exchange equilibrium of Ca and Mn between olivine and melt, $K_{D\ Ca\text{-}Mn}^{olivine/melt}$, passes through a minimum at NBO/T of the melt near 1. This NBO/T-value is near that where X_{Q3}/X_{Q2} has its largest value. Therefore, the activity coefficient ratio in the melt, $\gamma_{Ca^{2+}(melt)}/\gamma_{Mn^{2+}(melt)}$, reaches a minimum where the abundance ratio of X_{Q3}/X_{Q2} is at maximum. It is inferred from this relationship that Ca^{2+} in the melts is dominantly bonded to nonbridging oxygen in Q^3-species, whereas Mn^{2+} is bonded to nonbridging oxygen in less polymerized Q^n-species such as Q^2.

3. On the basis of the present data together with published data on $Fe^{2+} \Leftrightarrow Mg$ exchange between olivine and melt, as well as thermodynamic and structural data of melts and glasses from metal oxide-silica joins, it is proposed that the activity coefficients of major, minor, and trace elements in silicate melts can be correlated with the ionization potential, Z/r^2 of the cation. For a pair of network-modifying cations with different Z/r^2, i and j with $Z/r^2(j) > Z/r^2(i)$, exchange equilibrium constants between crystal and melt, $K_{D\ i\text{-}j}^{crystal/melt}$, will, therefore, exhibit a minimum at intermediate NBO/T of the melt. Interestingly, this NBO/T-value (~1) is near that of typical basalt melt (Mysen, 1988). This minimum $K_{D\ i\text{-}j}^{crystal/melt}$ exists because the ionization potential of cations i and j governs ordering of i and j among nonbridging oxygen in coexisting Q^n-species in the melt.

Acknowledgments—This research was partially supported by NSF grant EAR-9901886 and an REU grant to the Carnegie Institution of Washington. Thoughtful comments by Michael Carroll and Claudia Romano were particularly helpful.

Associate editor: C. Romano

REFERENCES

Alberto H. V., Pinto da Cunha J. L., Mysen B. O., Gil J. M., and de Campos N. A. (1996) Analysis of Mössbauer spectra of silicate glasses using a two-dimensional Gaussian distribution of hyperfine parameters. *J. Non-Cryst. Solids* **194,** 48–57.

Amthauer G., Langer K., and Schliestedt M. (1980) Thermally activated electron delocalization in deerite. *Phys. Chem. Minerals* **6,** 19–30.

Annersten H. (1976) New Mössbauer data on iron in potash feldspar. *N. Jb. Mineral.* **8,** 337–343.

Annersten H. and Olesch M. (1978) Distribution of ferrous and ferric iron in clintonite and the Mössbauer characteristics of ferric iron in tetrahedral coordination. *Can. Mineral.* **16,** 199–204.

Blundy J. D. and Wood B. J. (1994) Prediction of crystal-melt partition coefficients from elastic moduli. *Nature* **372,** 452–454.

Calas G., Levitz P., Petiau J., Bondot P., and Loupias G. (1980) Etude de l'ordre localautordu fer dans les verres silicates naturels et synthetiques a l'aide de la spectrometrie d'absorption. *X. Rev. Phys. Appl.* **15,** 1161–1167.

Calas G. and Petiau J. (1983) Coordination state of iron in oxide glasses through high-resolution K-edge spectra: Information from pre-edge. *Solid State Comm.* **48,** 625–629.

Colson R. O., McKay B. A., and Taylor L. A. (1988) Temperature and compostion dependencies of trace element partitioning: Olivine/melt and low-Ca pyroxene/melt. *Geochim. Cosmochim. Acta* **52,** 539–553.

Dingwell D. B. and Virgo D. (1987) The effect of oxidation state on the viscosity of melts in the system Na2O-FeO-Fe_2O_3-SiO_2. *Geochim. Cosmochim. Acta* **51,** 195–205.

Dingwell D. B. and Virgo D. (1988) Viscosities of melts in the Na2O-FeO-Fe_2O_3-SiO_2 systems and factors controlling relative viscosities in fully polymerized melts. *Geochim. Cosmochim. Acta* **52,** 395–404.

Fox K. E., Furukawa Y., and White W. B. (1982) Transition metal ions in silicate melts. Part 2. Iron in sodium silicate glasses. *Phys. Chem. Glasses* **23,** 169–178.

Hart S. R. and Davis K. E. (1978) Nickel partitioning between olivine and silicate melt. *Earth Planet. Sci. Lett.* **40,** 203–220.

Huebner J. S. (1969) The stability of rhodochrosite in the system manganese-carbon-hydrogen. *Am. Mineral.* **54,** 457–481.

Iiyama J. T. and Volfinger M. (1976) A model for trace element distribution in silicate structures. *Min. Mag.* **40,** 555–564.

Jaeger W. L. and Drake M. J. (2000) Metal-silicate partitioning of Co, Ga, and W: Dependence on silicate melt composition. *Geochim. Cosmochim. Acta* **64 (***22***),** 3887–3895.

Jones A. R., Winter R., Greaves G. N., and Smith I. H. (2001) MAS NMR study of soda-lime-silicate glasses with variable degrees of polymerisation. *J. Non-Cryst. Solids* **293-295,** 87–92.

Jurewicz A. J. G. and Watson E. B. (1988) Cations in olivine. Part I: Calcium partitioning and calcium-magnesium distribution between olivines and coexisting melts, with petrological applications. *Contr. Mineral. Petrol.* **99,** 176–185.

Kilinc A., Carmichael I. S. E., Rivers M. L., and Sack R. O. (1983) The ferric-ferrous ratio of natural silicate liquids equilibrated in air. *Contr. Mineral. Petrol.* **83,** 136–141.

Kohn S. C. and Schofield P. F. (1994) The importance of melt composition in controlling trace-element behaviour: An exprimental study of Mn and Zn partitioning between forsterite and silicate melt. *Chem. Geol.* **117,** 73–87.

Kushiro I. and Walter M. (1998) Mg-Fe Partitioning between olivine and mafic-ultramafic melts. *Geophys. Res. Lett.* **25,** 2337–2340.

Kushiro I. and Mysen B. O. (2002) A possible effect of melt structure on the Mg-Fe^{2+} partitioning between olivine and melt. *Geochim. Cosmochim. Acta* **66,** 2267–2273.

Lee S. K., Stebbins J. F., Mysen B. O. and Cody G. D. (2002) The nature of polymerization in silicate glasses and melts: Solid state NMR, modeling and quantum chemical calculations. *Eos* **83**(47).

Lee S. K. and Stebbins J. F. (2003) Nature of cation mixing and ordering in Na-Ca silicate glasses and melts. *J. Phys. Chem B* **107,** 3141–3148.

Libourel G. (1999) Systematics of calcium partitioning between olivine and silicate melt: Implications for melt structure and calcium content of magmatic olivines. *Contrib. Mineral. Petrol.* **136,** 63–80.

Liebau F. (1981) The influence of cation properties on the conformation of silicate and phosphate anions. In *Structure and Bonding in Crystals*, pp. 197–132. Academic Press.

Maekawa H., Maekawa T., Kawamura K., and Yokokawa T. (1991) The structural groups of alkali silicate glasses determined from ^{29}Si MAS-NMR. *J. Non-Cryst. Solids.* **127**(*1*), 53–64.

Mysen B. O. (1988) *Structure and Properties of Silicate Melts*. Elsevier.

Mysen B. O. (1990) Relationships between melt structure and petrologic processes. *Earth-Sci. Rev.* **27,** 261–365.

Mysen B. O. (1995) Experimental, in-situ, high-temperature studies of properties and structure of silicate melts relevant to magmatic temperatures. *Eur. J. Mineral.* **7,** 745–766.

Mysen B. O. (1997) Aluminosilicate melts: Structure, composition and temperature. *Contrib. Mineral. Petrol.* **127,** 104–118.

Mysen B. O. (1999) Structure and properties of magmatic liquids: From haplobasalt to haploandesite. *Geochim. Cosmochim. Acta* **63,** 95–112.

Mysen B. O. (2003) Physics and chemistry of silicate glasses and melts. *Eur. J. Mineral.* **15,** 781–802.

Mysen B. O. and Virgo D. (1980) Trace element partitioning and melt structure; an experimental study at 1 atm pressure. *Geochim. Cosmochim. Acta* **44** (*12*), 1917–1930.

Mysen B. O., Virgo D., and Seifert F. A. (1984) Redox equilibria of iron in alkaline earth silicate melts: Relationships between melt structure, oxygen fugacity, temperature and properties of iron-bearing silicate liquids. *Am. Mineral.* **69,** 834–848.

Mysen B. O., Virgo D., Neumann E. R., and Seifert F. A. (1985) Redox equilibria and the structural states of ferric and ferrous iron in melts in the system CaO-MgO-Al_2O_3-SiO_2: Relations between redox equilibria, melt structure and liquidus phase equilibria. *Am. Mineral.* **70,** 317–322.

Mysen B. O. and Virgo D. (1989) Redox equilibria, structure, and properties of Fe-bearing aluminosilicate melts: Relationships between temperature, composition, and oxygen fugacity in the system Na_2O-Al_2O_3-SiO_2-Fe-O. *Am. Mineral.* **74,** 58–76.

Mysen B. O. and Frantz J. D. (1994) Alkali silicate glass and melt structure in the temperature range 25–1651°C at atmospheric pressure and implications for mixing behavior of structural units. *Contrib. Mineral. Petrol.* **117,** 1–14.

Navrotsky A. (1995) Energetics of silicate melts. In *Structure, Dynamics and Properties of Silicate Melts*, Vol. 32 (eds. J. F. Stebbins, P. F. McMillan, and D. B. Dingwell). pp. 121–146. Mineralogical Society of Ameria.

Navrotsky A., Geisinger K. L., McMillan P., and Gibbs G. V. (1985) The tetrahedral framework in glasses and melts—Influences from molecular orbital calculations and implications for structure, thermodynamics, and physical properties. *Phys. Chem. Minerals* **11,** 284–298.

Osborn E. F. and Arculus R. J. (1975) Phase relations in the system Mg_2SiO_4-iron oxide-$CaAl_2Si_2O_8$-SiO_2 at 10 kbar and their bearing on the origin of andesite. *Carnegie Inst. Wash. Year Book* **74,** 504–507.

Ryerson F. J. (1985) Oxide solution mechanisms in silicate melts: Systematic variations in the activity coefficient of SiO_2. *Geochim. Cosmochim. Acta* **49,** 637–651.

Sato M. (1972) Electrochemical measurements and control of oxygen fugacity and other gaseous fugacities with solid electrolyte system. In *Research Techniques for High Pressure and High Temperature* (ed. G. C. Ulmer), chap. 3. Springer Verlag.

Schramm C. M., DeJong B. H. W. S., and Parziale V. F. (1984) ^{29}Si magic angle spinning NMR study of local silicon environments in-amorphous and crystalline lithium silicates. *J. Am. Chem. Soc.* **106,** 4396–4402.

Schwerdtfeger K. and Muan A. (1966) Activities in olivine and pyroxenoid solid solutions of the system Fe-Mn-Si-O at 1150°C. *Trans. Metallurg. Soc. AIME* **236,** 201–211.

Spiering B. and Seifert F. A. (1985) Iron in silicate glasses of granitic composition: A Mössbauer spectroscopic investigation. *Contrib. Mineral. Petrol.* **90,** 63–73.

Stebbins J. F. (1987) Identification of multiple structural species in silicate glasses by ^{29}Si NMR. *Nature* **330,** 465–467.

Toplis M. J. and Corgne A. (2002) An experimental study of element partitioning between magnetite, clinopyroxene and iron-bearing silicate liquids with particular emphasis on vanadium. *Contrib. Mineral. Petrol.* **144,** 22–37.

Virgo D., Mysen B. O., and Kushiro I. (1980) Anionic constitution of 1-atmosphere silicate melts: Implications of the structure of igneous melts. *Science* **208,** 1371–1373.

Virgo D. and Mysen B. O. (1985) The structural state of iron in oxidized vs. reduced glasses at 1 atm: A ^{57}Fe Mössbauer study. *Phys. Chem. Minerals* **12,** 65–76.

Walter M. J. (2001) Core formation in a reduced magma ocean: New constraints from W, P, Ni and Co. In *Transport of Materials in the Dynamic Earth*, pp. 152–153.

Warner R. D. and Luth W. C. (1974) The diopside-orthoenstatite two-phase region in the system $CaMgSi_2O_6$-$Mg_2Si_2O_6$. *Am. Mineral.* **59,** 98–109.

Watson E. B. (1976) Partitioning of manganese between forsterite and liquid. *Eos* **57** (*4*), 339.

Watson E. B. (1977) Partitioning of manganese between forsterite and silicate liquid. *Geochim. Cosmochim. Acta* **41,** 1363–1374.

Waychunas G. A. and Rossman G. R. (1983) Spectroscopic standard for tetrahedrally-coordinated ferric iron: gammaLiAlO_2:Fe^{3+}. *Phys. Chem. Minerals* **9,** 212–215.

Whittaker E. J. W. and Muntus R. (1970) Ionic radii for use in geochemistry. *Geochim. Cosmochim. Acta* **34,** 945–957.

Wilke M., Behrens H., Burkhard D. J. M., and Rossano S. (2002) The oxidation state of iron in silicic melt at 500 MPa water pressure. *Earth Planet. Sci. Lett.* **189,** 55–67.

Wood B. J. and Blundy J. D. (2001) The effect of cation charge on crystal-melt partitioning of trace elements. *Earth Planet. Sci. Lett.* **188,** 59–71.